

Validation of Ionospheric Specifications During Geomagnetic Storms: TEC and foF2 during the 2013 March Storm Event-II

Ja Soon Shim¹, In-Sun Song², Geonhwa Jee³, Young-Sil Kwak⁴, Ioanna Tsagouri⁵, Larisa Goncharenko⁶, Joseph McInerney⁷, Francis Vitt⁷, Lutz Rastaetter⁸, Jia Yue⁹, Min-Yang Chou⁹, Mihail V. Codrescu¹⁰, Anthea J Coster¹¹, Mariangel Fedrizzi¹², Timothy J. Fuller-Rowell¹³, Aaron J. Ridley¹⁴, and Stanley C. Solomon⁷

¹Yonsei University,

²Yonsei University

³Korea Polar Research Institute

⁴Korea Astronomy and Space Science Institute

⁵National Observatory of Athens

⁶MIT Haystack Observatory, Westford, MA, USA.

⁷National Center for Atmospheric Research (UCAR)

⁸NASA/GSFC

⁹Goddard Space Flight Center

¹⁰Space Weather Prediction Center, National Oceanic And Atmospheric Administration

¹¹MIT Haystack Observatory

¹²University of Colorado/CIRES and NOAA/SWPC

¹³NOAA Space Weather Prediction Center

¹⁴University of Michigan-Ann Arbor

December 18, 2022

Abstract

Assessing space weather modeling capability is a key element in improving existing models and developing new ones. In order to track improvement of the models and investigate impacts of forcing, from the lower atmosphere below and from the magnetosphere above, on the performance of ionosphere-thermosphere models, we expand our previous assessment for 2013 March storm event [Shim et al., 2018]. In this study, we evaluate new simulations from upgraded models (Coupled Thermosphere Ionosphere Plasmasphere Electrodynamics (CTIpe) model version 4.1 and Global Ionosphere Thermosphere Model (GITM) version 21.11) and from NCAR Whole Atmosphere Community Climate Model with thermosphere and ionosphere extension (WACCM-X) version 2.2 including 8 simulations in the previous study. A simulation of NCAR Thermosphere-Ionosphere-Electrodynamics General Circulation Model version 2 (TIE-GCM 2) is also included for comparison with WACCM-X. TEC and foF2 changes from quiet-time background are considered to evaluate the model performance on the storm impacts. For evaluation, we employ 4 skill scores: Correlation coefficient (CC), root-mean square error (RMSE), ratio of the modeled to observed maximum percentage changes (Yield), and timing error (TE). It is found that the models tend to underestimate the storm-time enhancements of foF2 (F2-layer critical frequency) and TEC (Total Electron Content) and to predict foF2 and/or TEC better in the North America but worse in the Southern Hemisphere. The ensemble simulation for TEC is comparable to results from a data assimilation model (Utah State University-Global Assimilation of Ionospheric Measurement (USU-GAIM)) with differences in skill score less than 3% and 6% for CC and RMSE, respectively.

23 **Key Points:**

- 24 • foF2/TEC and their changes during a storm predicted by seven ionosphere-thermosphere
25 coupled models are evaluated against GIRO foF2 and GPS TEC measurements.
- 26 • Model simulations tend to underestimate the storm-time enhancements of foF2 and TEC
27 and to predict them better in the North America but worse in the southern hemisphere.
- 28 • Ensemble of all simulations for TEC is comparable to the data assimilation model (USU-
29 GAIM).
- 30

31 **Abstract**

32 Assessing space weather modeling capability is a key element in improving existing models and
33 developing new ones. In order to track improvement of the models and investigate impacts of
34 forcing, from the lower atmosphere below and from the magnetosphere above, on the
35 performance of ionosphere-thermosphere models, we expand our previous assessment for 2013
36 March storm event [*Shim et al.*, 2018]. In this study, we evaluate new simulations from upgraded
37 models (Coupled Thermosphere Ionosphere Plasmasphere Electrodynamics (CTIPE) model
38 version 4.1 and Global Ionosphere Thermosphere Model (GITM) version 21.11) and from
39 NCAR Whole Atmosphere Community Climate Model with thermosphere and ionosphere
40 extension (WACCM-X) version 2.2 including 8 simulations in the previous study. A simulation
41 of NCAR Thermosphere-Ionosphere-Electrodynamics General Circulation Model version 2
42 (TIE-GCM 2) is also included for comparison with WACCM-X. TEC and foF2 changes from
43 quiet-time background are considered to evaluate the model performance on the storm impacts.
44 For evaluation, we employ 4 skill scores: Correlation coefficient (CC), root-mean square error
45 (RMSE), ratio of the modeled to observed maximum percentage changes (Yield), and timing
46 error(TE). It is found that the models tend to underestimate the storm-time enhancements of foF2
47 (F2-layer critical frequency) and TEC (Total Electron Content) and to predict foF2 and/or TEC
48 better in the North America but worse in the Southern Hemisphere. The ensemble simulation for
49 TEC is comparable to results from a data assimilation model (Utah State University-Global
50 Assimilation of Ionospheric Measurement (USU-GAIM)) with differences in skill score less than
51 3% and 6% for CC and RMSE, respectively.

52

53 **Plain Language Summary**

54 The Earth's ionosphere-thermosphere (IT) system, which is present between the lower
55 atmosphere and the magnetosphere, is highly variable due to external forcings from below and
56 above as well as internal forcings mainly associated with ion-neutral coupling processes. The
57 variabilities of the IT system can adversely affect our daily lives, therefore, there is a need for
58 both accurate and reliable weather forecasts to mitigate harmful effects of space weather events.
59 In order to track the improvement of predictive capabilities of space weather models for the IT
60 system, and to investigate the impacts of the forcings on the performance of IT models, we
61 evaluate new simulations from upgraded models (CTIPe model version 4.1 and GITM version
62 21.11) and from NCAR WACCM-X version 2.2 together with 8 simulations in the previous
63 study. A simulation of NCAR TIE-GCM version 2 is also included for the comparison with
64 WACCM-X. Quantitative evaluation is performed by using 4 skill scores including Correlation
65 coefficient (CC), root-mean square error (RMSE), ratio of the modeled to observed maximum
66 percentage changes (Yield), and timing error (TE). The findings of this study will provide a
67 baseline for future validation studies of new and improved models.

68

69 **1. Introduction**

70 Variabilities of the Earth's ionosphere-thermosphere (IT) system, caused by charged
71 particles and electromagnetic radiation emitted from the sun, can adversely affect our daily lives,
72 which are highly dependent on space-based technological infrastructures such as Low-Earth
73 Orbit (LEO) satellites and the Global Navigation Satellite System (GNSS). To mitigate harmful
74 effects of space weather events, modeling plays a critical role in our quest to understand the
75 connection between solar eruptive phenomena and their impacts in interplanetary space and near-
76 Earth space environment. In particular, the Earth's upper atmosphere including the IT system is

77 the space environment closest to the human society. Thus, during the past few decades, first-
78 principles physics-based (PB) IT models have been developed for specifications and forecasts of
79 the near-Earth space environment. In addition, there have been recent developments of whole
80 atmosphere models with thermospheric and ionospheric extension to fully understand
81 variabilities of the IT system by considering coupling between the IT system and the lower
82 atmosphere [e.g., *Akmaev*, 2011; *Fuller-Rowell et al.*, 2010; *Jin et al.*, 2011; *Liu et al.*, 2018].

83 For more accurate space weather forecasting, assessing space weather modeling capability is
84 a key element to improve existing models and to develop new models. Over the last decade, in
85 an effort to address the needs and challenges of the assessment of our current knowledge about
86 space weather effects on the IT system and current state of IT modeling capabilities, the NASA
87 GSFC Community Coordinated Modeling Center (CCMC) has been supporting community-wide
88 model validation projects, including Coupling, Energetics and Dynamics of Atmospheric
89 Regions (CEDAR) [*Shim et al.*, 2011, 2012, 2014] and Geospace Environment Modeling
90 (GEM)-CEDAR modeling challenges [*Rastätter et al.*, 2016; *Shim et al.*, 2017a].

91 Furthermore, in 2018, the CCMC established an international effort, “International Forum
92 for Space Weather Modeling Capabilities Assessment”, to evaluate and assess the predictive
93 capabilities of space weather models (<https://ccmc.gsfc.nasa.gov/iswat/IFSWCA/>). As a result of
94 this international effort, four ionosphere/thermosphere working groups were established with an
95 overarching goal to devise a standardized quantitative validation procedure for IT models
96 [*Scherliess et al.*, 2019].

97 The working group, focusing on neutral density and orbit determination at LEO, reported
98 their initial results for specific metrics for thermosphere model assessment over the selected
99 three full years and two geomagnetic storms in 2005 [*Bruinsma et al.*, 2018]. They reported that

100 the tested models in general performed reasonably well, although seasonal errors were
101 sometimes observed and impulsive geomagnetic events remain a challenge. Kalafatoglu Eyigüler
102 et al. (2019) compared the neutral density estimates from two empirical and three PB models
103 with those obtained from the CHAMP satellite. They suggested that several metrics that provide
104 different aspects of the errors should be considered together for a proper performance evaluation.

105 Another working group, “Ionosphere Plasmasphere Density Working Team”, performed the
106 assessment of present modeling capabilities in predicting the ionospheric climatology of f_0F_2
107 and hmF_2 for the entire year 2012 [Tsaygouri et al., 2018]. Tsaygouri et al. (2018) identified a
108 strong seasonal and local time dependence of the model performances, especially for PB models,
109 which could provide useful insight for future model improvements. Tsaygouri et al. cautioned that
110 the quality of the ground truth data may play a key role in testing the model performance. Shim
111 et al. (2018) assessed how well the ionospheric models predict storm time f_0F_2 and TEC by
112 considering quantities, such as TEC and f_0F_2 changes and percentage changes compared to quiet
113 time background, at 12 selected midlatitude locations in the American and European-African
114 longitude sectors. They found that the performance of the model varies with locations, even
115 within a localized region like Europe, as well as with the metrics considered.

116 In this paper, we expand our previous assessment of modeled f_0F_2 and TEC during 2013
117 March storm event (17 March, 2013) [Shim et al., 2018] to track improvement of the models and
118 to investigate impacts of forcings from the lower atmosphere below and from the magnetosphere
119 above on the performance of IT models. For this study, we evaluate the updated version of the
120 coupled IT models available at the CCMC [Webb et al., 2009] since our previous study [Shim et
121 al., 2018]: CTIPe version 4.1 and GITM version 21.11. However, the other types of models such
122 as empirical models, stand-alone ionospheric models, and data assimilation models are not

123 included. In addition, for the first time, simulations of NCAR WACCM-X 2.2 are included in
124 our assessment. We also included a simulation of NCAR TIE-GCM 2 to compare with results
125 from WACCM-X 2.2. For TEC prediction, we compare a weighted mean of the ensemble of all
126 13 simulations (ensemble average), including 8 simulations from our previous study with
127 individual simulations to assess ensemble forecast capability. In Section 2, we briefly describe
128 observations, models, and metrics used for this study. Section 3 presents the results of model-
129 data comparisons and performance of the models are presented. Section 4 shows comparisons of
130 ensemble of TEC predictions with the individual simulations based on the skill scores used in
131 this study. Finally, we summarize and conclude in Section 5.

132

133 **2. Methodology**

134 **2.1 Observations and Metrics**

135 We use the foF2 and TEC measurements at 12 ionosonde stations selected in middle
136 latitudes: 8 northern hemisphere (NH) stations in the US (Millstone Hill, Idaho national Lab,
137 Boulder, and Eglin AFB) and Europe (Chilton, Pruhonice, Ebre, and Athens) and 4 southern
138 hemisphere (SH) stations in South America (Port Stanley) and South Africa (Louisvale,
139 Hermanus, and Grahamstown) (Figure 1 and Table 1 in *Shim et al.* [2018] for details). The foF2
140 and GNSS vertical TEC (vTEC) data are provided by Global Ionosphere Radio Observatory
141 (GIRO) (<http://giro.uml.edu/>) [*Reinisch and Galkin*, 2011] and by MIT Haystack Observatory
142 (<http://cedar.openmadrigal.org/>, <http://cedar.openmadrigal.org/cgi-bin/gSimpleUIAccessData.py>)
143 [*Rideout and Coster*, 2006], respectively.

144 Table 1 shows the quantities and skill scores calculated for model-data comparison. To
145 remove potential systematic uncertainties in the models and observations and baseline

146 differences among the models and between models and observations, we use the shifted values
147 and changes from their own quiet-time background values (e.g., shifted TEC (TEC^*) = TEC
148 (UT) on a particular DOY – median (UT) of TEC for 30 days centered on the storm date).
149 Furthermore, using these quantities likely reduce the impacts of differing upper boundaries for
150 TEC calculations, since the plasmaspheric TEC variations with geomagnetic activity are
151 negligible in middle latitudes [*Shim et al.*, 2017b].

152 To measure how well the observed and modeled values are linearly correlated (in phase)
153 with each other and how different the values are on average over the time interval considered,
154 CC and RMSE are calculated, respectively, for the error values below 95th percentile. We also
155 calculate Yield and timing error to measure the models' capability to capture peak disturbances
156 during the storm. For more detailed information on the quantities and skill scores used for the
157 study, refer to Section 2 in *Shim et al.* [2018].

158

159 **2.2 Models and Simulations**

160 The simulations used in this study are obtained from the updated and newly incorporated
161 coupled ionosphere-thermosphere models available at the CCMC [*Webb et al.*, 2009] since our
162 previous study [*Shim et al.*, 2018]: CTIPe 4.1, GITM 21.11 and WACCM-X 2.2. The WACCM-
163 X 2.2 simulations are provided by NCAR HAO. The WACCM-X version 2 [*Liu et al.*, 2018] is a
164 comprehensive numerical model that extends the atmospheric component model of the NCAR
165 Community Earth System Model (CESM) [*Hurrell et al.*, 2013] into the thermosphere up to
166 500–700 km altitude. WACCM-X is uniquely capable of being run in a configuration where the
167 atmosphere is coupled to active or prescribed ocean, sea ice, and land components, enabling
168 studies of thermospheric and ionospheric weather and climate. WACCM-X version 2 is based

169 upon WACCM version 6 [Gettelman *et al.*, 2019] with a top boundary of ~130 km, which is
170 built upon the Community Atmosphere Model (CAM) version 6 having a top boundary of ~40
171 km. WACCM-X 2.2 includes WACCM6 physics for middle atmosphere and lower thermosphere
172 as well as CAM6 physics for the troposphere and the lower stratosphere, and it fully incorporates
173 the electrodynamical processes related to low-to mid-latitude wind dynamo that is implemented
174 in the NCAR TIE-GCM. For this study, two specified-dynamics (SD) WACCM-X 2.2
175 simulations with different high-latitude electrostatic potential models [Heelis *et al.*, 1982;
176 Weimer, 2005] are used. The SD simulations are carried out by constraining the model's lower
177 atmospheric neutral dynamics using meteorological reanalysis data. The constraining process is
178 achieved by nudging the model towards MERRA-2 (Modern Era Retrospective Analysis for
179 Research and Applications, Version 2) data [Gelaro *et al.*, 2017] below around the altitude of 50
180 km in a way presented by Brakebusch *et al.* [2013].

181 The resulting WACCM-X simulations are compared with the simulations of TIE-GCM. The
182 comparisons between WACCM-X and TIE-GCM simulations will show differences and
183 similarities in modeling capabilities between whole atmosphere modeling and ionosphere-
184 thermosphere modeling with a specified low-boundary forcing (e.g., Global Scale Wave Model
185 (GSWM) [Hagan *et al.*, 1999] used for this study).

186 Table 2 shows the version of the models, input data used for the simulations, and models
187 used for lower boundary forcing and high latitude electrodynamics. We utilized unique model
188 setting identifiers to distinguish the current simulations from those used in our previous studies
189 [Shim *et al.*, 2011, 2012, 2014, 2017a, 2018]. Additional information for the models and model
190 setting identifiers is available in Shim *et al.* [2011] (Refer to all references therein) and at
191 https://ccmc.gsfc.nasa.gov/support/GEM_metrics_08/tags_list.php

192 To investigate improvement in foF2 and TEC predictions of the updated versions of CTIPE
193 (12_CTIPE) and GITM (7_GITM), the simulations of the old versions of the models (11_CTIPE
194 and 6_GITM) from our previous study are included. The comparison will be focused on the
195 comparison between the simulations obtained from the same model. As for TIE-GCM, 12_TIE-
196 GCM (run at 2.5° resolution) is presented for this study, but the comparison between
197 11_TIE_GCM and 12_TIE-GCM was not included in this study because the only difference
198 between the two is horizontal resolution (5°lat.×5°long. vs 2.5°lat.×2.5°long.).

199 We should take note of the difference between the simulations obtained from the same
200 model that influence foF2 and TEC responses to geomagnetic storms. For two CTIPE runs,
201 different lower atmospheric tides were specified: 11_CTIPE was driven by the imposed
202 migrating semidiurnal (2,2), (2,3), (2,4), (2,5), and diurnal (1,1) tidal modes, while 12_CTIPE
203 was run with monthly mean spectrum of tides obtained from WAM (Whole Atmosphere Model)
204 [Akmaev *et al.*, 2011, Fuller-Rowell *et al.*, 2010]. For two GITM simulations, 7_GITM used
205 Fang's auroral precipitation [Fang *et al.*, 2013], while 6_GITM used Ovation model [Newell *et*
206 *al.*, 2009; 2011]. For two WACCM-X simulations, Heelis and Weimer2005 electric potential
207 models were used for 3_WACCM-X and 4_WACCM-X, respectively. 12_TIEGCM was driven
208 by Weimer2005 electric potential model and GSWM.

209

210 **3. Performance of the Models in Predictions of foF2 and vTEC on 17 March 2013**

211 Most simulations newly added for this study show similar behavior to those used in Shim *et*
212 *al.* [2018], in predicting foF2 and TEC during the storm. For example, the simulations are not
213 able to reproduce (1) the difference between eastern and western parts of the North American
214 sector (e.g., TEC increases at Millstone Hill but decreases at Idaho and Boulder around 20UT),

215 and (2) different responses between foF2 (negligible changes) and TEC (noticeable increase)
216 found in European (Chilton) and South-African (Grahamstown) stations (See Figure 4 of Shim et
217 al. [2018] for reference). However, compared to other simulations, 4_WACCM-X driven by
218 *Weimer* (2005) high latitude electric potential model captures relatively well the two differences
219 in TEC and foF2 described above (Figure S1 in supporting information).

220 Figure 1 shows scatter plots of the observed (*x* axis) and modeled (*y* axis) shifted foF2 and
221 TEC, and percentage change of foF2 and TEC during the storm (03/17/2013) for all 12 locations
222 grouped into 4 sectors: North America (NA, green), Europe (EU, blue), South Africa (SAF, red),
223 and South America (SAM, black). First of all, the qualitative comparison between the
224 simulations from the same model can be summarized as follows. 11_CTIPE/12_CTIPE tends to
225 underestimate foF2 for both quiet and disturbed conditions, but 12_CTIPE predicts much better
226 both foF2 and TEC during the storm than 11_CTIPE. 6_GITM and 7_GITM underestimate foF2
227 and TEC for all cases and show relatively small response to the storm compared to the other
228 simulations. 12_TIE-GCM and WACCM-Xs produce similar foF2 and TEC changes during the
229 storm. All three simulations give *substantial underestimation of TEC in SAF*. 12_TIE-GCM and
230 3_WACCM-X produce larger overestimation of foF2 and TEC in NA sector than 4_WACCM-X.
231 4_WACCM-X shows substantial improvement in the TEC overestimation in NA. 3_WACCM-X,
232 of which the high latitude electric potential is specified by Heelis et al. [1982], tends to
233 overestimate foF2 and TEC compared with 4_WACCM-X. 3_WACCM-X and 4_WACCM-X
234 produce better quiet time foF2 and TEC than 12_TIEGCM does and capture wave-like small
235 increases in foF2 and TEC at Idaho National Lab around 10–11UT (2–3 LT) (Figure S1 in
236 supporting information).

237 As shown for 6_GITM and 11_CTIPE in *Shim et al.* [2018], the modeled foF2 values of
238 7_GITM and 12_CTIPE better agrees with the observed ones when they are shifted by
239 subtracting the minimum of 30-day median (see Figure S2 in supporting information, *Shim et al.*
240 [2018]). Most foF2 and TEC data points of 7_GITM and 12_CTIPE before shifting are below
241 and above the line with slope 1 (black solid line), respectively. This indicates that 7_GITM
242 underestimates foF2 and TEC like 6_GITM, while 12_CTIPE overestimates them. The models
243 that tend to underestimate foF2, such as 6_GITM, 7_GITM and 11_CTIPE, seem to unable to
244 produce foF2* larger than about 7 MHz, and underestimate TEC* being less than about 20
245 TECU during the storm as reported in *Shim et al.* [2018]. 12_TIE-GCM and WACCM-Xs show
246 similar distribution of the data points after shifting foF2 and TEC with a tendency to
247 underestimate foF2 and TEC in the South Africa region.

248 The modeled dfoF2[%] and dTEC[%] show less agreement with the observed values than
249 the modeled foF2* and TEC* do. The data points in the 2nd quadrant (top left) and the 4th
250 quadrant (bottom right) indicate that the modeled and observed percentage changes are in
251 opposite sign. 7_GITM and 3_WACCM-X have more data points in the 2nd quadrant for
252 dfoF2[%] prediction than 6_GITM and 4_WACCM-X, respectively. Like most simulations used
253 in our previous evaluation [*Shim et al.* 2018], 12_CTIPE and 7_GITM do not appear to
254 reproduce the large dTEC[%] (about 200 %) at Port Stanley in SAM. However, 12_TIE-GCM
255 and WACCM-Xs better produce the enhancement in TEC percentage change. Compared to
256 4_WACCM-X and 12_TIE-GCM, 3_WACCM-X overestimates dTEC[%] especially in NA and
257 EU regions. 12_CTIPE and 6_GITM have more data points of overestimated dTEC[%] in SAF
258 than 11_CTIPE and 7_GITM, respectively.

259 From now on, foF2 and TEC will represent shifted foF2 (foF2*) and shifted TEC (TEC*),
260 respectively.

261

262 **3.1 Correlation Coefficient (CC)**

263 We first calculate correlation coefficient (CC) between the modeled and observed foF2 and
264 TEC for DOY 076 (17 March, 2013) for quantitative assessment of the model performance of
265 TEC and foF2 predictions. In Figure 2, the CCs for each simulation are presented for foF2 in the
266 left panel and for TEC in the right panel. For each simulation, four CC values are displayed. First
267 three of the values correspond to the average CC over Europe (EU), North America (NA),
268 Southern Hemisphere (SH refers to SAF and SAM combined), and the last one is the average of
269 all 12 locations. The modeled foF2 and TEC (blue dots) are highly correlated with the observed
270 values. The average CC values over all 12 locations for both foF2 and TEC are about 0.8–0.95,
271 but the average CCs for their changes are much smaller. For example, the CCs for TEC changes
272 (dTEC) are 0.5–0.6 and even smaller for foF2. The modeled foF2 changes (green), percentage
273 changes (red) and normalized percentage changes (black only applicable for TEC) are much less
274 correlated (closer to uncorrelated) with the observed values (about $0.1 < \text{average CC} < 0.4$).
275 There is no big difference between dTEC[%] and dTEC[%]_norm based on the average values
276 for each simulation as reported in *Shim et al.* [2018].

277 Note that the CC values for the changes and percentage changes of foF2 and TEC are highly
278 dependent on locations. Most simulations, except for 12_CTIPE and GITMs, show lower CC for
279 dfoF2 and dTEC in NA. It seems to be caused by the decreases of foF2 and TEC during the
280 storm (negative phase) in the western parts of NA that are not captured well. GITMs show the

281 negative phase well although it underestimated the magnitude of the change. The CCs for the
282 percentage changes of foF2 and TEC are particularly small for CTIPEs and GITMs.

283 11_CTIPe's foF2 and TEC averaged over 12 locations are slightly better correlated with the
284 observed values than 12_CTIPe. However, the changes and percentage changes of foF2 and
285 TEC from 12_CTIPe are better correlated with the observed values than 11_CTIPe's values in
286 most regions. Although the two GITMs produce similar CCs, 7_GITM shows better CC in NA
287 regions for dfoF2, dfoF2[%], dTEC[%], and n_dTEC[%], while 6_GITM shows better CC for
288 foF2 and dTEC. WACCM-Xs perform better than 12_TIE_GCM for all the considered quantities
289 based on the average except for dTEC. WACCM-Xs perform similar to each other.

290 Close inspection of Figures. 1 and 2 indicates that a linearity between CTIPe and
291 observations is improved in the newer version of CTIPe (12_CTIPe), but 12_CTIPe gives more
292 scattered distribution around a linear relation (Fig. 1), which seems to lead to the lower CC in
293 12_CTIPe than in 11_CTIPe. 7_GITM exhibits a slight improvement in a linearity between the
294 model and observations (Fig. 1), but this improvement is not clearly seen in the correlation
295 analysis (Fig. 2). For 12_TIEGCM and WACCM-Xs, both a linearity between the models and
296 observations (Fig. 1) and CCs (Fig. 2) demonstrate that the model performances are overall
297 improved in WACCM-Xs compared with TIEGCM. In terms of the model-observation linearity,
298 4_WACCMX is somewhat better than 3_WACCMX (Fig. 1), but their CCs seems comparable to
299 each other (Fig. 2).

300

301 **3.2 Root Mean Square Error (RMSE)**

302 Figure 3 shows RMSE of foF2 and dfoF2 in the left panel, and TEC and dTEC in the right
303 panel. For foF2 (blue) and dfoF2 (green) predictions, based on the average RMSE values, the

304 RMSEs from the updated version (12_CTIPE and 7_GITM) are about 1.5 MHz for foF2 and
305 about 1 MHz for dfoF2, and they are slightly lower than RMSEs in their old versions. 12_CTIPE
306 shows improvement in foF2 in SH and dfoF2 in NA and EU compared to 11_CTIPE. 7_GITM
307 performs better in foF2 and dfoF2 in EU and SH than 6_GITM. 4_WACCM-X has smaller
308 RMSE (~1 MHz) than 3_WACCM-X and 12_TIE-GCM (~1.3 MHz for dfoF2 and ~2 MHz for
309 foF2).

310 12_CTIPE is better in TEC prediction than 11_CTIPE, while the opposite holds true for
311 dTEC prediction. The two GITMs' average RMSE values for TEC and dTEC predictions are
312 similar to each other, about 9 TECU for TEC and 5 TECU for dTEC. Like foF2 and dfoF2
313 prediction, 4_WACCM-X has smaller RMSE (~ 5 TECU for TEC and 4 TECU for dTEC) than
314 12_TIE-GCM and 3_WACCM-X (~6 TECU).

315 As seen in *Shim et al.* [2018], RMSE is highly variable with location. Most simulations
316 appear to predict foF2 and/or TEC better in NA and worse in SH (except for 12_TIE-GCM for
317 foF2 and 12_CTIPE for TEC). Both 11_CTIPE and GITMs tend to perform better in NA for
318 dTEC, while WACCM-Xs show the opposite tendency for dfoF2 and dTEC. 7_GITM and
319 4_WACCM-X shows the least RMSE dependence on location for dfoF2 and for dTEC,
320 respectively, among seven simulations.

321 Figure 4 shows the RMSE of percentage changes of foF2 (blue) and TEC (red) and
322 normalized percentage changes of TEC (black). The two CTIPEs produce the similar RMSE for
323 dTEC[%], but 12_CTIPE and 11_CTIPE produce lower RMSE for dfoF2[%] and
324 dTEC[%]_norm, respectively. For all three percentage changes of dfoF2[%], dTEC[%], and
325 dTEC[%]_norm, 7_GITM seems to perform better than 6_GITM based on the average RMSEs

326 over the 12 locations. 4_WACCM-X and 12_TIE-GCM perform very similarly for dfoF2[%] and
327 dTEC[%] and better than 3_WACCM-X.

328 Difference in the performance among locations is more noticeable in dTEC[%] and
329 dTEC[%]_norm than in dfoF2[%] as found in *Shim et al.* [2018]. All simulations, except
330 6_GITM, produce lower RMSE of dTEC[%] in NA and higher in SH region. This tendency
331 remains the same for dTEC[%]_norm with the exception of 3_WACCM-X, which has lower
332 RMSE for dTEC[%]_norm in SH. For 3_WACCM-X, the higher RMSE for dTEC[%] and the
333 lower RMSE for dTEC[%]_norm in SH than in NA are probably due to the normalization factor,
334 standard deviation of dTEC[%] in the locations.

335

336 **3.3 Yield and Timing Error (TE)**

337 To measure how well the models capture the degree of TEC and foF2 disturbances during
338 the main phase, Yield and Timing Error (TE) of dfoF2[%], dTEC[%], and dTEC[%]_norm are
339 calculated. *Shim et al.* [2018] considered two time intervals, 06–15UT and 15–22UT, when
340 peaks are observed in most of 12 locations. In each time interval, we calculate one Yield value
341 and one TE value. Definitions of Yield and TE are presented in Table 1.

342 In each sector, average Yield and TE are calculated over the number of stations where the
343 model correctly predicts the storm phase, i.e., Yield is positive. Table 3 shows the total number
344 of stations where the models show correct storm phase, either positive or negative. The numbers
345 in bold are the higher values between the simulations compared. 12_CTIPE predicts the storm
346 phase better for dTEC[%] than 11_CTIPE, but 11_CTIPE predicts better for dfoF2[%] than
347 12_CTIPE. 7_GITM is improved in predicting the storm phase of dfoF2[%], while 6_GITM
348 predicts better the storm phase of dTEC[%]. 4_WACCM-X, compared to 12_TIE-GCM and

349 3_WACCM-X, is better for predicting the phase of dfoF2[%] and worse for predicting that of
 350 dTEC[%].

351 Figure 5 shows average Yield (left) and average of absolute values of TE (right) over the
 352 two time intervals: dfoF2[%] in blue, dTEC[%] in red, and dTEC[%]_norm in black. Concerning
 353 the average of all 12 locations, 12_CTIPE appears to overestimate peak values of dTEC[%] and
 354 dTEC[%]_norm with larger variation with location (e.g., $\sim 1 < \text{Yield of dTEC[\%]_norm} < \sim 2.5$)
 355 than 11_CTIPE, of which Yield is less than 1 for all three quantities of percentage changes (e.g.,
 356 $0.7 < \text{Yield of dTEC[\%]_norm} < 0.9$). Yields of 12_CTIPE for dTEC[%] and dTEC[%]_norm
 357 are closer to 1 in NA. GITMs produce similar ratios based on the average over all locations, but
 358 7_GITM shows smaller differences in Yield among locations (e.g., $\sim 0.5 < \text{Yield of}$
 359 $\text{dTEC[\%]_norm} < \sim 1$) than 6_GITM (e.g., $0.5 < \text{Yield of dTEC[\%]_norm} < \sim 2.5$). In terms of
 360 average Yield, 12 TIE-GCM and two WACCM-Xs tend to overestimate the peak values and
 361 show similar performance, although 12_TIE-GCM's ratios are closer to 1 than those of
 362 WACCM-Xs. 3_WACCM-X shows larger variation in Yield among locations (e.g., $\sim 0.9 < \text{Yield}$
 363 $\text{of dTEC[\%]_norm} < \sim 2.7$) than 12_TIE-GCM and 4_WACCM-X (e.g., $\sim 1.7 < \text{Yield of}$
 364 $\text{dTEC[\%]_norm} < \sim 2.3$).

365 Average Timing Errors of dfoF2[%] and dTEC[%]_norm are between 1 and 2 hours, and
 366 TE of dTEC[%] are about 0.8–1.5 hours. With respect to the average TE, 12_CTIPE has smaller
 367 TE (~ 1 hr) than 11_CTIPE (about 1.5 hr) for all three percentage changes with less location
 368 dependence as well. 7_GITM's three TEs are about 1.5 hrs, while 6_GITM's TEs of dfoF2[%],
 369 dTEC[%] and dTEC[%]_norm are ~ 1 , ~ 1.4 , and ~ 2 hrs, respectively. 12 TIE-GCM has smaller
 370 TE for dfoF2[%] and 3_WACCM-X has smaller TE for dTEC[%] and dTEC[%]_norm, however
 371 3_WACCM-X show larger location dependence of TE for dTEC[%]_norm and dfoF2[%].

372

373 **4. Ensemble of TEC obtained from 13 simulations**

374 The linearity check, RMSE, and CC between model results and observations for shifted foF2
375 and TEC and their relative changes indicate that the newer versions of the models (i.e.,
376 12_CTIPE, 7_GITM and 4_WACCM-X) produces the better results. From the viewpoints of
377 correct prediction of storm phases (Table 3), Yields, and TEs (Fig. 5), however, there is no one
378 best simulation for all locations, and the performance of model varies with locations as well as
379 the Yields and TE.

380 The differences in performance among the simulations could be caused by inherent
381 differences among the models or by a combination of different input data and different models
382 used for lower boundary forcing and high-latitude electrodynamics. Even different data
383 assimilation models for the same weather condition can yield different results, due to numerous
384 reasons (e.g., the use of different background weather models, spatial/temporal resolutions,
385 assimilation methods, and data error analyses), even if the same data are assimilated [*Schunk et*
386 *al.*, 2021]. The common way to handle these differences is to use model ensembles and the use
387 of ensembles enables estimations of the certainty of results. Thus, we used a weighted mean of
388 the ensemble of all 13 simulations including 8 simulations from our previous study (*Shim et al.*,
389 2018) for TEC, dTEC and dTEC[%] to compare the ensemble average with the individual
390 simulations. To get the weighted mean ($\bar{x} = \sum w_i x_i / \sum w_i$), we used the RMSE of shifted TEC
391 ($w_i = 1/\text{RMSE}$).

392 Figure 6 is the same as Figure 1 but for the ensemble of the simulations (ENSEMBLE will
393 be used as model setting ID) and a simulation (1_USU-GAIM) from a data assimilation model
394 (DA), USU-GAIM. For TEC less than about 20 TECU, ENSEMBLE shows better agreement

395 with GPS TEC than the individual simulations, including 1_USU-GAIM. However, as we can
396 expect, ENSEMBLE underestimates TEC larger than about 30 TECU due to the tendency to
397 underestimate TEC of many simulations as pointed out in Section 3 and *Shim et al.*, [2018]. For
398 dTEC[%], ENSEMBLE appears to be correlated better with GPS dTEC[%] than the other
399 simulations, although there are some underestimations in SAF, as well as in SAM with opposite
400 prediction of the storm phase.

401 Figure 7 shows averaged CC and RMSE values over all 12 locations of 13 simulations, the
402 ensemble of them, and the ensemble of 12 simulations excluding 1_USU-GAIM
403 (ENSEMBLE_wo_DA). The simulations in Figure 7 (a) were arranged by the average of the
404 three averaged CC values for TEC, dTEC and dTEC[%] from the smallest to the largest (closer
405 to 1). In Figure 7 (b), the simulations were arranged by the average of the two averaged RMSEs
406 for TEC and dTEC from the largest to the smallest. Based on the averaged CC and RMSE,
407 ENSEMBLES (ENSEMBLE and ENSEMBLE_wo_DA) of the simulations perform very
408 similarly and outperform all 12 simulations but a data assimilation model, 1_USU-GAIM.
409 However, ENSEMBLES and 1_USU-GAIM do not show big difference in their performance.
410 The differences in RMSE of TEC and dTEC between ENSEMBLE and 1_USU-GAIM are less
411 than 0.5 and 0.1 TECU, respectively. For dTEC[%], ENSEMBLE performs slightly better than
412 1_USU-GAIM with about 1.5% lower RMSE. The fact that ENSEMBLES are comparable to the
413 data assimilation model 1_USU-GAIM indicates that the multi-model ensemble can be useful in
414 forecasting the IT system, although this result is obtained from a single geomagnetic storm event.

415 Figure 8 shows Yield and Timing Error of dTEC[%] for all 13 simulations along with
416 ENSEMBLE. The values correspond to the average over all 12 locations. Unlike CC and RMSE,
417 ENSEMBLE does not outperform all physic-based coupled models in terms of Yield and TE,

418 although the difference is small. ENSEMBLE underestimates Yield, while most of the
419 simulations overestimate it, except 4_IRI and 11_CTIPE. 7 simulations from PB coupled IT
420 models and 1_USU-GAIM produce Yield closer to 1 than ENSEMBLE does.

421 Timing Error of dTEC[%] of ENSEMBLE is about 1 hr, which is slightly larger than TE
422 from 4 simulations from CTIPE and WACCM-X, but the difference from the smallest TE is less
423 than 0.5 hr.

424 Regarding the averaged skill scores for all 12 locations, newly added five simulations in this
425 study produce comparable TEC and TEC changes to the simulations from PB IT models used in
426 our previous study. The simulations of newer versions of the models (12_CTIPE, 7_GITM and
427 4_WACCM-X) are found to give overall improved forecast results. Based on the averaged
428 RMSE, the ensemble of simulations of the models' newer versions is comparable to 1_USU-
429 GAIM and performs better than the ensemble of the simulations of old versions of models
430 (11_CTIPE, 6_GITM and 12_TIE-GCM) (Table 4).

431

432 **5. Summary and Conclusions**

433 We expanded on our previous systematic assessment of modeled foF2 and TEC during
434 2013 March storm event (17 March, 2013) to track the improvement of the models and
435 investigate impacts of forcings from the lower atmosphere and the magnetosphere, on the
436 performance of ionosphere-thermosphere coupled models.

437 We evaluated simulations from upgraded models (CTIPE4.1 and GITM21.11) since our
438 previous assessment and a whole atmosphere model (WACCM-X2.2). To compare with results
439 from WACCM-X2.2, we also included a simulation of TIE-GCM2.0, of which the
440 electrodynamic processes are implemented in WACCM-X 2.2. Furthermore, to evaluate TEC

441 prediction of the simulations, we used a weighted mean of the ensemble of all 13 simulations
442 including 8 simulations from our previous study to compare the ensemble average with the
443 individual simulations.

444 For evaluation of the simulations, we used the exact same procedure with the same data set,
445 same physical quantities, and same skill scores as our previous study [*Shim et al.*, 2018]. The
446 skill scores were calculated for the three sectors, EU (Europe), NA (North America), and SH
447 (Southern Hemisphere) to investigate the longitudinal and hemispheric dependence of the
448 performance of the models.

449 From the five simulations used in the study, we also found the general behaviors of most
450 simulations identified in *Shim et al.* [2018]: 1) tendency to underestimate storm-time
451 enhancements of foF2 and TEC and not to reproduce large enhancements of dTEC[%] (e.g.,
452 about 200 % TEC increase at Port Stanley in the SAA region), 2) being unable to capture
453 opposite responses to the storm in the eastern and western parts of NA, especially negative phase
454 (except for GITM), which is what in part causes lower CC in NA, 3) tendency to predict foF2
455 and/or TEC better in NA and worse in SH with respect to RMSE. However, it was found that
456 12_TIE-GCM and WACCM-Xs better produce the large TEC percentage changes at Port Stanley
457 in SAM. Based on the averaged skill scores for all 12 locations, the five simulations used in this
458 study show skill scores better or comparable to those of the simulations from PB IT models used
459 in our previous study.

460 Compared to 11_CTIPE (obtained from CTIPe3.2), 12_CTIPE (from CTIPe4.1) driven by
461 tides from WAM tends to overestimate foF2 and TEC for both quiet and disturbed conditions
462 and predicts better TEC peaks during the storm. For more cases, 12_CTIPE performs largely
463 better than 11_CTIPE based on the average scores. 12_CTIPE predicts the storm phase better for

464 dTEC[%], but 11_CTIPE does better for dfoF2[%]. 12_CTIPE appears to overestimate peak
465 values of dTEC[%] and dTEC[%]_norm, while 11_CTIPE produces Yield less than 1.

466 The two GITMs, 7_GITM with Fang's auroral precipitation and 6_GITM with Ovation
467 model, underestimate foF2 and TEC for all cases and show relatively small response to the storm
468 compared to the other simulations that do not appear to reproduce the large dTEC[%] (about
469 200 % increase at Port Stanley in SAM). 7_GITM and 6_GITM perform very similarly for most
470 cases with similar skill scores. However, 7_GITM shows better CC for most quantities except for
471 dTEC, and lower RMSEs and Yield closer to 1 for most regions and quantities considered.
472 7_GITM shows the least RMSE dependence on location for dfoF2 among the other simulations.

473 Comparing two WACCM-Xs and 12_TIE-GCM, the two WACCM-Xs, 3_WACCM-X with
474 Heelis high latitude electric potential model and 4_WACCM-X with Weimer 2005, predict quiet
475 time foF2 and TEC better than 12_TIE-GCM. During the storm, 12_TIE-GCM and 4_WACCM-
476 X produce similar foF2 and TEC in NA sector, while 3_WACCM-X tends to overestimate them
477 and produces larger changes in foF2 and TEC. In most cases, WACCM-Xs and 12_TIE_GCM
478 perform similarly in terms of average values of skill scores, but 3_WACCM-X and/or
479 4_WACCM-X perform better than 12_TIE-GCM except for Yield of percentage changes.
480 4_WACCM-X slightly outperforms 3_WACCMX for all cases but not for TE for percentage
481 changes.

482 Our findings suggest that the newer versions of the models (12_CTIPE, 7_GITM and
483 4_WACCM-X) with Weimer2005 electric potential model give overall improved forecast, and
484 the performance of the models depends on forcing from the magnetosphere and also forcing from
485 the lower atmosphere even during storms.

486 For TEC, dTEC and dTEC[%], our results indicate that the ensemble of all 13 simulations
487 (ENSEMBLE), including 8 simulations from our previous study (*Shim et al.*, 2018) is
488 comparable to the data assimilation model (1_USU-GAIM) with differences in skill score less
489 than 3% and 6% for CC and RMSE, respectively. However, ENSEMBLE underestimates Yield
490 (0.73) while 7 simulations from PB coupled IT models and 1_USU-GAIM produce Yield closer
491 to 1. Timing Error of dTEC[%] of ENSEMBLE is about 1 hr, but the difference from the
492 smallest TE of the simulations is less than 0.5 hr. In addition, based on RMSE, the ensemble of
493 the newer versions of the models (12_CTIPE, 7_GITM and 4_WACCM-X) is comparable to
494 1_USU-GAIM.

495 To advance our understanding of the ionosphere-thermosphere system requires significant
496 efforts to improve the capability of numerical models along with the scope of observations
497 [*Heelis and Maute*, 2020]. There have been recent new developments of theoretical models,
498 including AMGeO (Assimilative Mapping of Geospace Observations) for High-Latitude
499 Ionospheric Electrodynamics [*Matsuo*, 2020] and MAGE geospace model that couples the Grid
500 Agnostic MHD for Extended Research Applications (GAMERA) global MHD model of
501 the magnetosphere (Sorathia et al., 2020; Zhang et al., 2019), the Rice Convec-tion Model
502 (RCM) model of the ring current (Toffoletto et al., 2003), TIEGCM of the upper atmosphere and
503 the RE-developed Magnetosphere-Ionosphere Coupler/Solver (REMIX) (Merkin & Lyon, 2010).
504 These models will be available soon to the public through CCMC, and then the modeling
505 capability will help us better understand the processes responsible for the observed
506 characteristics and features during disturbed conditions. In addition, CCMC will also provide
507 users with the capability to run PB IT models with various combination of models for lower

508 atmospheric forcing and for magnetosphere forcing, which enable us to research further the
509 impacts of the forcings on the IT system.

510 The findings of this study will provide a baseline for future validation studies using new
511 models and improved models, along with earlier results [*Shim et al.*, 2011, 2012, 2014, 2017a,
512 2018] obtained through CEDAR ETI, GEM-CEDAR Modeling Challenges, and the international
513 effort, “International Forum for Space Weather Modeling Capabilities Assessment”. We will
514 extend our study to include more geomagnetic storm events to investigate differences and
515 similarities in the performance of the models. In addition, we will also include foF2 and TEC
516 predictions for the high- and low-latitude regions.

517

518 **Acknowledgement**

519 This work was supported by Korea Polar Research Institute (KOPRI) grant funded by the
520 Ministry of Oceans and Fisheries (KOPRI PE22020) and basic research funding from the Korea
521 Astronomy and Space Science Institute (KASI) (KASI2022185009). The vertical TEC data were
522 provided by MIT Haystack Observatory and can be obtained through CEDAR Madrigal database
523 (<http://cedar.openmadrigal.org>). We thank the operators of the digisondes for sharing their data
524 through <http://giro.uml.edu/>. Data from the South African Ionosonde network is made available
525 through the South African National Space Agency (SANSA), who are acknowledged for
526 facilitating and coordinating the continued availability of data. This work is supported by grants
527 from the National Science Foundation (NSF) Space Weather Program. This model validation
528 study is supported by the Community Coordinated Modeling Center (CCMC) at the Goddard
529 Space Flight Center. Data processing and research at MIT Haystack Observatory are supported
530 by cooperative agreement AGS-1242204 between the U.S. National Science Foundation and the

531 Massachusetts Institute of Technology. The National Center for Atmospheric Research is
532 sponsored by the National Science Foundation. Model output and observational data used for the
533 study will be permanently posted at the CCMC website (<http://ccmc.gsfc.nasa.gov>) and provided
534 as a resource for the space science community to use in the future.

535

536

537 **References**

538 Akmaev, R. A. (2011). Whole atmosphere modeling: Connecting terrestrial and space weather.
539 *Reviews of Geophys.* 49, RG4004. 390 <https://doi.org/10.1029/2011RG000364>

540 Brakebusch, M., Randall, C. E., Kinnison, D. E., Tilmes, S., Santee, M. L., and Manney, G. L.
541 (2013) Evaluation of Whole Atmosphere Community Climate Model simulations of ozone
542 during Arctic winter 2004–2005, *J. Geophys. Res.*, 118, 2673–2688,
543 <https://doi.org/10.1002/jgrd.50226>

544 Bruinsma, S., Sutton, E., Solomon, S. C., Fuller-Rowell, T., & Fedrizzi, M. (2018). Space
545 weather modeling capabilities assessment: Neutral density for orbit determination at low Earth
546 orbit. *Space Weather*, 16, 1806–1816. <https://doi.org/10.1029/2018SW002027>

547

548 Chamberlin, P. C., Woods, T. N., & Eparvier, F. G. (2007). Flare Irradiance Spectral Model
549 (FISM): Daily component algorithms and results. *Space Weather*, 5, S07005.
550 <https://doi.org/10.1029/2007SW000316>

- 551 Codrescu, M. V., T. J. Fuller-Rowell, J. C. Foster, J. M. Holt, and S. J. Cariglia, (2000), Electric
552 field variability associated with the Millstone Hill electric field model, *J. Geophys. Res.*, 105,
553 5265–5273, doi:10.1029/1999JA900463.
- 554 Fang, X., D. Lummerzheim, and C. H. Jackman (2013), Proton impact ionization and a fast
555 calculation method, *J. Geophys. Res. Space Physics*, 118, 5369–5378, doi:10.1002/jgra.50484.
- 556 Fuller -Rowell, T. J., and D. S. Evans, (1987), Height-Integrated Pedersen and Hall Conductivity
557 Patterns Inferred From the TIROS-NOAA Satellite Data, *J. Geophys. Res.*, 92(A7), 7606–7618.
- 558 Fuller-Rowell, T., Wu, F., Akmaev, R., Fang, T.-W., & Araujo-Pradere, E. (2010). A whole
559 atmosphere model simulation of the impact of a sudden stratospheric warming on thermosphere
560 dynamics and electrodynamics. *Journal of Geophysical Research*, 115, A00G08. [https://](https://doi.org/10.1029/2010JA015524)
561 doi.org/10.1029/2010JA015524
- 562 Gelaro, R., McCarty, W., Suárez, M. J., Todling, R., Molod, A., Takacs, L., et al. (2017). The
563 Modern-Era Retrospective Analysis for Research and Applications, version 2 (MERRA-2).
564 *Journal of Climate*, 30(14), 5419–5454. <https://doi.org/10.1175/JCLI-D-16-0758.1>
- 565 Gettelman, A., Mills, M. J., Kinnison, D. E., Garcia, R. R., Smith, A. K., Marsh, D. R., et
566 al.(2019). The whole atmosphere community climate model version 6 (WACCM6), *Journal of*
567 *Geophysical Research: Atmospheres*, 124, 12,380–12,403. [https://doi.org/](https://doi.org/10.1029/2019JD030943)
568 [10.1029/2019JD030943](https://doi.org/10.1029/2019JD030943).
- 569 Hagan, M. E., M. D. Burrage, J. M. Forbes, J. Hackney, W. J. Randel, and X. Zhang, (1999),
570 GSWM-98: results for migrating solar tides. *J. Geophys. Res.* 104: 6813–6828.

- 571 Hedin, A. E. (1991), Extension of the MSIS thermospheric model into the middle and lower
572 atmosphere, *J. Geophys. Res.*, 96, 1159–1172.
- 573 Heelis, R. A., J. K. Lowell, and R. W. Spiro, (1982), A Model of the High-Latitude Ionospheric
574 Convection Pattern, *J. Geophys. Res.* 87, 6339.
- 575 Heelis, R. A., & Maute, A. (2020). Challenges to understanding the Earth's ionosphere and
576 thermosphere. *JGR: Space Physics*, 125, [https:// doi.org/10.1029/2019JA027497](https://doi.org/10.1029/2019JA027497)
- 577 Jin, H., Miyoshi, Y., Fujiwara, H., Shinagawa, H., Terada, K., Terada, N., et al. (2011). Vertical
578 connection from the tropospheric activities to the ionospheric longitudinal structure simulated by
579 a new Earth's whole atmosphere-ionosphere coupled model. *Journal of Geophysical Research*,
580 116, A01316. <https://doi.org/10.1029/2010JA015925>
- 581 Kalafatoglu Eyiguler, E. C., Shim, J. S., Kuznetsova, M. M., Kaymaz, Z., Bowman, B. R.,
582 Codrescu, M. V., et al. (2019). Quantifying the storm time thermospheric neutral density
583 variations using model and observations. *Space Weather*, 17, 269–284.
584 <https://doi.org/10.1029/2018SW002033>.
- 585 Liu, H.-L., Bardeen, C. G., Foster, B. T., Lauritzen, P., Liu, J., Lu, G., . . . Wang, W. (2018). Development
586 and validation of the Whole Atmosphere Community Climate Model with thermosphere and ionosphere
587 extension (WACCM-X 2.0), *Journal of Advances in Modeling Earth Systems*, 10. [https://doi.org/10.1002/](https://doi.org/10.1002/2017MS001232)
588 2017MS001232
- 589
- 590 Matsuo, T. (2020). Recent Progress on Inverse and Data Assimilation Procedure for High-
591 Latitude Ionospheric Electrodynamics. In: Dunlop, M., Lühr, H. (eds) *Ionospheric Multi-*

- 592 Spacecraft Analysis Tools. ISSI Scientific Report Series, vol 17. Springer, Cham.
593 https://doi.org/10.1007/978-3-030-26732-2_10
- 594 Merkin, V., & Lyon, J. (2010). Effects of the low-latitude ionospheric boundary condition on the
595 global magnetosphere. *Journal of Geophysical Research*, 115(A10). A10202.
596 <https://doi.org/10.1029/2010JA015461>
- 597 Millward, G. H., I. C. F. Müller-Wodrag, A. D. Aylward, T. J. Fuller-Rowell, A. D. Richmond,
598 and R. J. Moffett, (2001), An investigation into the influence of tidal forcing on F region
599 equatorial vertical ion drift using a global ionosphere-thermosphere model with coupled
600 electrodynamics, *J. Geophys. Res.*, 106, 24,733–24,744, doi:10.1029/2000JA000342.
- 601 Newell, P. T., T. Sotirelis, and S. Wing (2009), Diffuse, monoenergetic, and broadband aurora:
602 The global precipitation budget, *J. Geophys. Res.*, 114, A09207, doi: 10.1029/2009JA014326.
603
- 604 Newell, P.T., and J.W. Gjerloev (2011), Substorm and magnetosphere characteristic scales
605 inferred from the SuperMAG auroral electrojet indices, *J. Geophys. Res.*, 116, A12232,
606 doi:10.1029/2011JA016936.
- 607 Rastätter, L., et al., (2016), GEM-CEDAR Challenge: Poynting Flux at DMSP and modeled
608 Joule Heat, *Space Weather*, 14, 113–135, doi:10.1002/2015SW001238.
- 609 Reinisch, B., and I. Galkin, (2011). Global Ionospheric Radio Observatory (GIRO). *Earth,*
610 *Planets, and Space*. 63. 377-381. 10.5047/eps.2011.03.001.

- 611 Richmond, A. D., E. C. Ridley and R. G. Roble, (1992), A Thermosphere/Ionosphere General
612 Circulation Model with coupled electrodynamics, *Geophys. Res. Lett.*, **19**, 601-604.
- 613 Rideout, W., and A. Coster, (2006), Automated GPS processing for global total electron content
614 data, GPS Solution, doi:10.1007/s10291-006-0029-5.
- 615 Ridley, A. J., Y. Deng, and G. Toth, (2006), The global ionosphere-thermosphere model, *J.*
616 *Atmos. Sol. Terr. Phys.*, **68**, 839-864.
- 617 Roble, R. G., E. C. Ridley, A. D. Richmond, and R. E. Dickinson, (1988), A coupled
618 thermosphere/ionosphere general circulation model, *Geophys. Res. Lett.*, **15**, 1325–1328,
619 doi:10.1029/GL015i012p01325.
- 620 Scherliess, L., Tsagouri, I., Yizengaw, E., Bruinsma, S., Shim, J. S., Coster, A., and Retterer, J.
621 M. (2019). The International Community Coordinated Modeling Center space weather modeling
622 capabilities assessment: Overview of ionosphere/thermosphere activities. *Space Weather*, **17**.
623 [https:// doi.org/10.1029/2018SW002036](https://doi.org/10.1029/2018SW002036)
- 624 Schunk, R. W., Scherliess, L., Eccles, V., Gardner, L. C., Sojka, J. J., Zhu, L., et al. (2021).
625 Challenges in specifying and predicting space weather. *Space Weather*, **19**, e2019SW002404.
626 [https:// doi.org/10.1029/2019SW002404](https://doi.org/10.1029/2019SW002404)
- 627 Shim, J. S., et al., (2011), CEDAR Electrodynamics Thermosphere Ionosphere (ETI) Challenge
628 for systematic assessment of ionosphere/thermosphere models: NmF2, hmF2, and vertical drift
629 using ground-based observations, *Space Weather*, **9**, S12003, doi:10.1029/2011SW000727.

630 Shim, J. S., et al., (2012), CEDAR Electrodynamic Thermosphere Ionosphere (ETI) Challenge
631 for systematic assessment of ionosphere/thermosphere models: Electron density, neutral density,
632 NmF2, and hmF2 using space based observations, *Space Weather*, 10, S10004,
633 doi:10.1029/2012SW000851.

634 Shim, J. S., et al., (2014), Systematic Evaluation of Ionosphere/Thermosphere (IT) Models:
635 CEDAR Electrodynamic Thermosphere Ionosphere (ETI) Challenge (2009-2010), in *Modeling*
636 *the Ionosphere-Thermosphere System*, AGU Geophysical Monograph Series.

637 Shim, J. S., Rastätter, L., Kuznetsova, M., Bilitza, D., Codrescu, M., Coster, A. J., ... Zhu, L.
638 (2017a). CEDAR-GEM challenge for systematic assessment of Ionosphere/thermosphere models
639 in predicting TEC during the 2006 December storm event. *Space Weather*, 15, 1238–1256.
640 <https://doi.org/10.1002/2017SW001649>

641

642 Shim, J. S., G. Jee, and L. Scherliess (2017b), Climatology of plasmaspheric total electron
643 content obtained from Jason 1 satellite, *J. Geophys. Res. Space Physics*, 122, 1611–1623,
644 doi:10.1002/2016JA023444.

645

646 Shim, J. S., Tsagouri, I., Goncharenko, L., Rastaetter, L., Kuznetsova, M., Bilitza, D., et al.
647 (2018). Validation of ionospheric specifications during geomagnetic storms: TEC and foF2
648 during the 2013 March storm event. *Space Weather*, 16, 1686–1701. [https://doi.org/10.1029/](https://doi.org/10.1029/2018SW002034)
649 [2018SW002034](https://doi.org/10.1029/2018SW002034)

650

- 651 Solomon, S. C., A. G. Burns, B. A. Emery, M. G. Mlynczak, L. Qian, W. Wang, D. R. Weimer,
652 and M. Wiltberger (2012). Modeling studies of the impact of high-speed streams and co-rotating
653 interaction regions on the thermosphere-ionosphere. *J. Geophys. Res.*, *117*, A00L11,
654 doi:10.1029/2011JA017417
- 655 Sorathia, K., Merkin, V., Panov, E., Zhang, B., Lyon, J., Garretson, J., et al. (2020). Ballooning-
656 interchange instability in the near-Earth plasma sheet and auroral beads: Global magnetospheric
657 modeling at the limit of the MHD approximation. *Geophysical Research Letters*, *47*(14),
658 e2020GL088227. <https://doi.org/10.1029/2020GL088227>
- 659 Tsagouri, I., Goncharenko, L., Shim, J. S., Belehaki, A., Buresova, D., & Kuznetsova, M.
660 (2018). Assessment of current capabilities in modeling the ionospheric climatology for space
661 weather applications: foF2 and hmF2. *Space Weather*, *16*, 1930–1945.
662 <https://doi.org/10.1029/2018SW002035>
- 663 Toffoletto, F., Sazykin, S., Spiro, R., & Wolf, R. (2003). Inner magnetospheric modeling with
664 the rice convection model. *Space Science Reviews*, *107*(1–2), 175–196.
665 <https://doi.org/10.1023/A:1025532008047>
- 666 Webb, P. A., M. M. Kuznetsova, M. Hesse, L. Rastaetter, and A. Chulaki, (2009), Ionosphere-
667 thermosphere models at the Community Coordinated Modeling Center, *Radio Sci.*, *44*, RS0A34,
668 doi:10.1029/2008RS004108.
- 669 Weimer, D. R., (2005), Improved ionospheric electrodynamic models and application to
670 calculating Joule heating rates, *J. Geophys. Res.*, *110*, A05306, doi:10.1029/2004JA010884.

- 671 Zhang, B., Sorathia, K. A., Lyon, J. G., Merkin, V. G., Garretson, J. S., & Wiltberger, M. (2019).
672 GAMERA: A three-dimensional finite-volume MHD solver for non-orthogonal curvilinear
673 geometries. *The Astrophysical Journal Supplement Series*, 244(1), 20.
674 <https://doi.org/10.3847/1538-4365/ab3a4c>

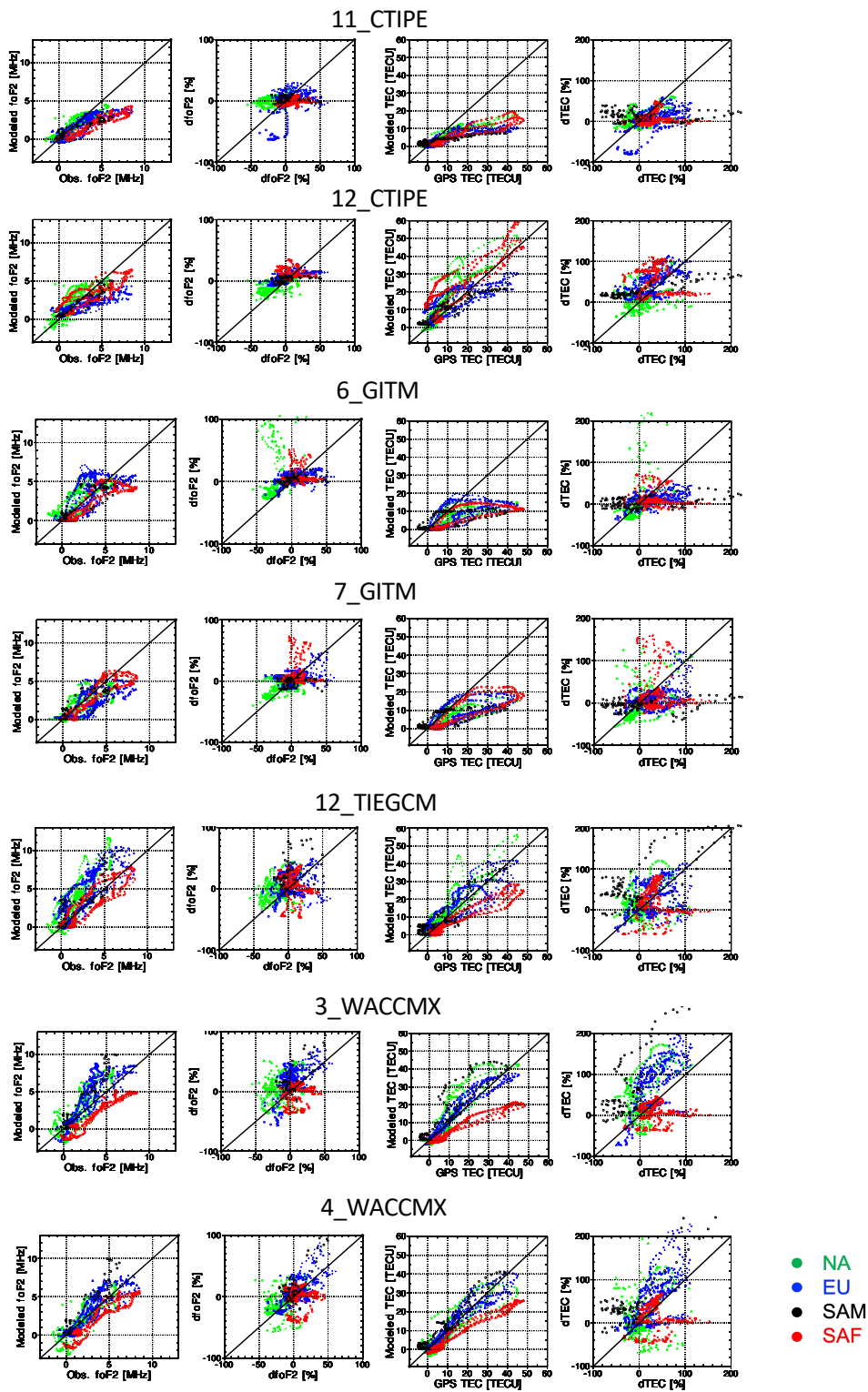


Figure 1

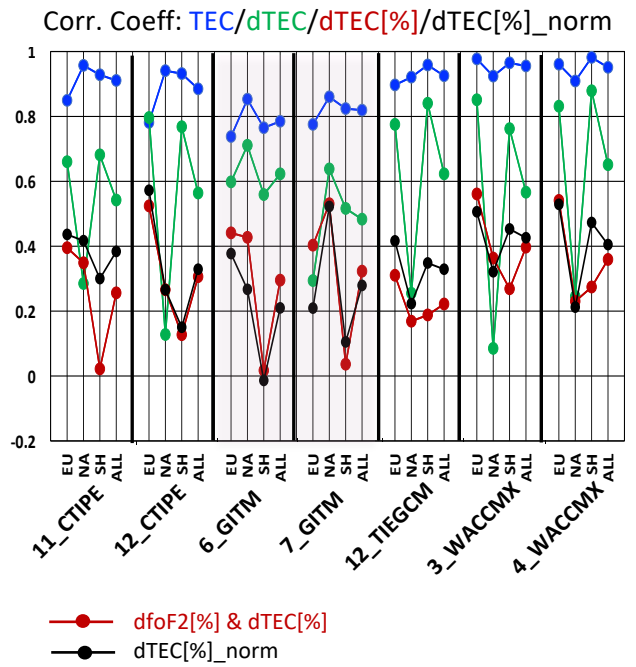
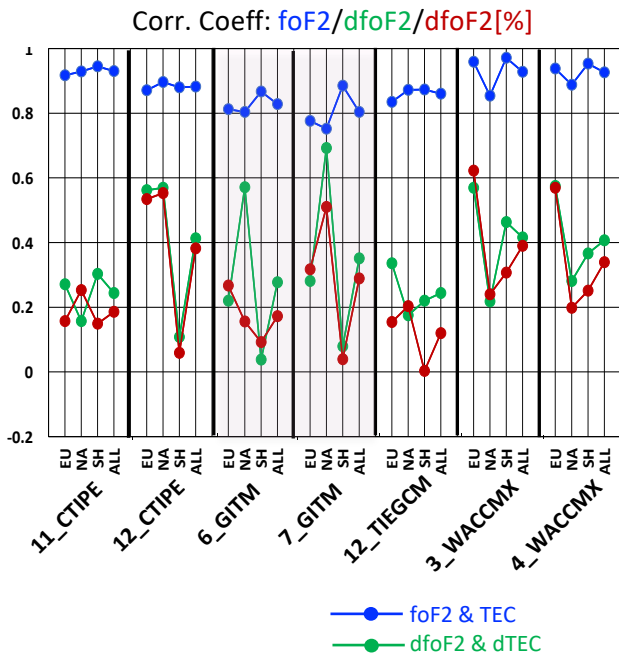
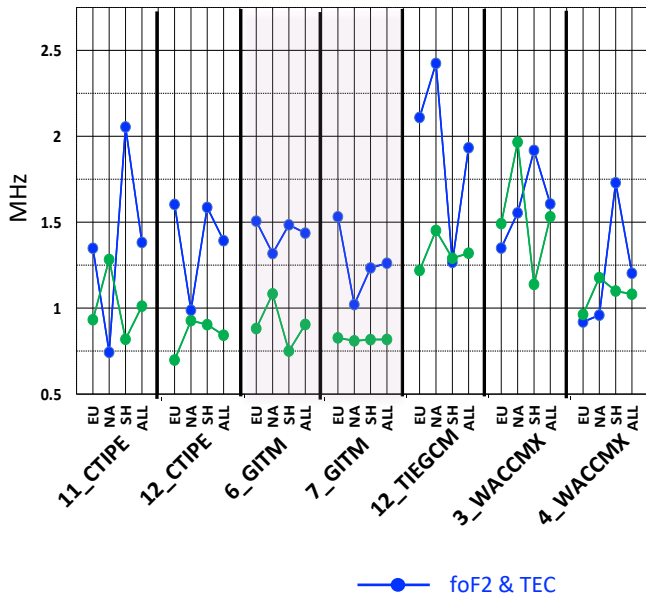


Figure 2

RMSE: foF2/dfoF2



RMSE: TEC/dTEC

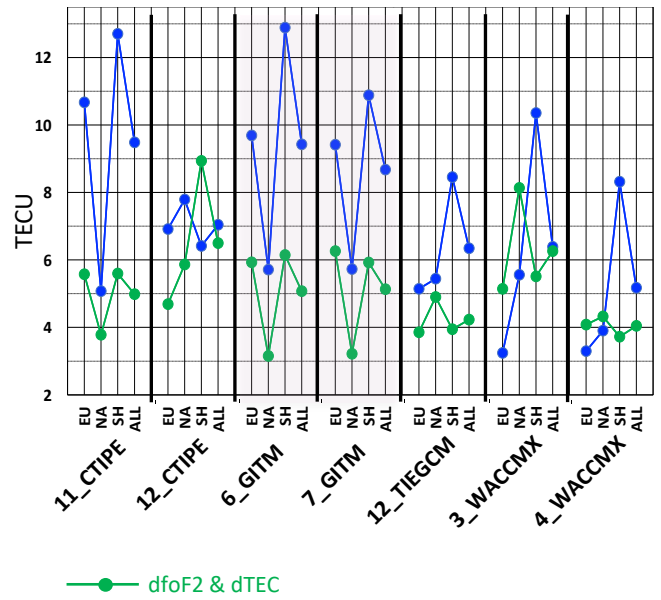


Figure 3

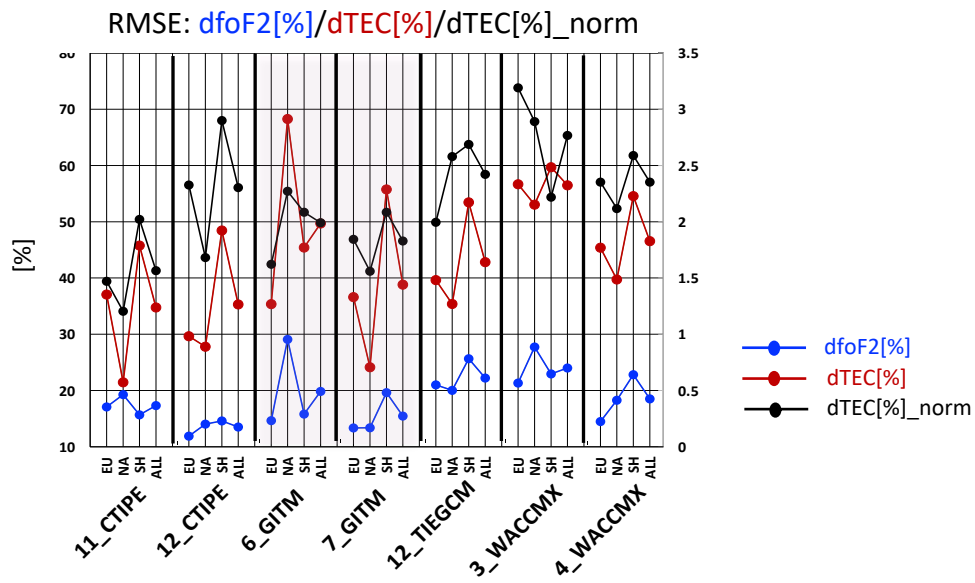


Figure 4

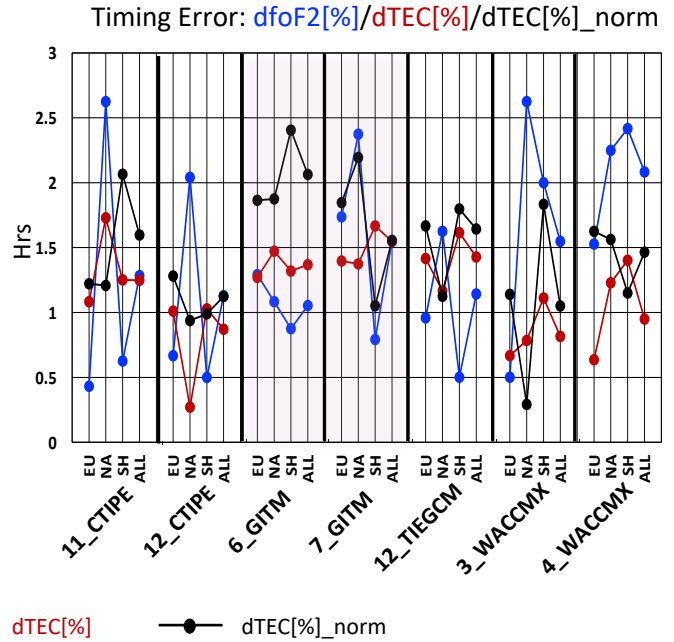
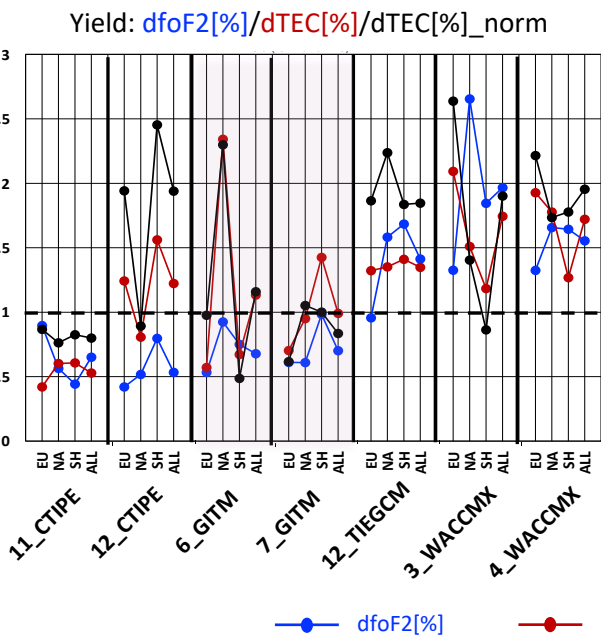


Figure 5

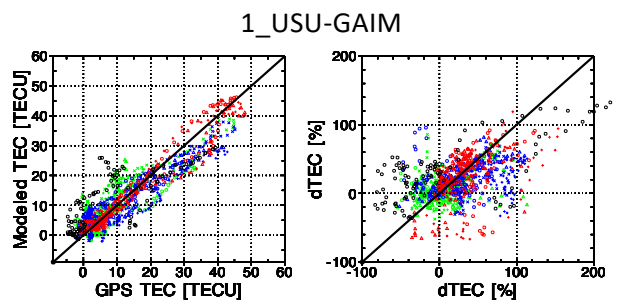
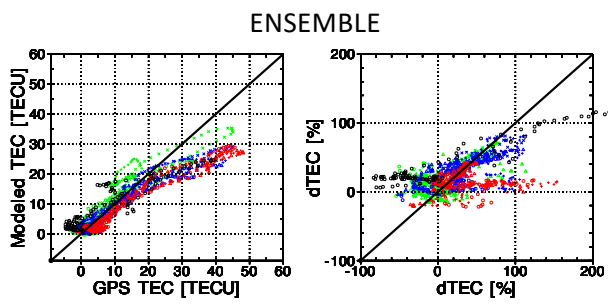


Figure 6

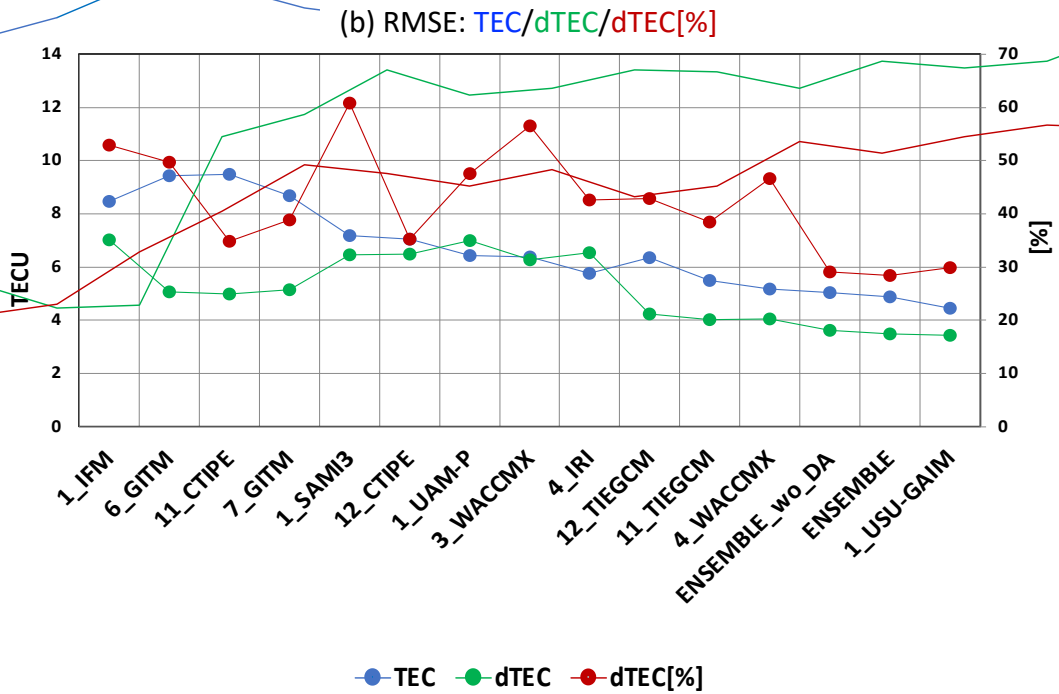
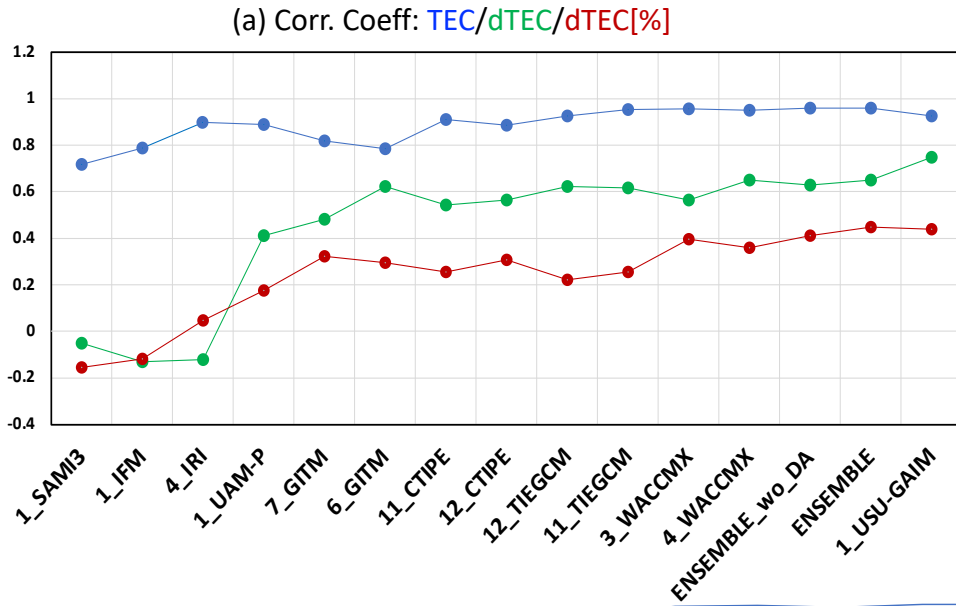


Figure 7

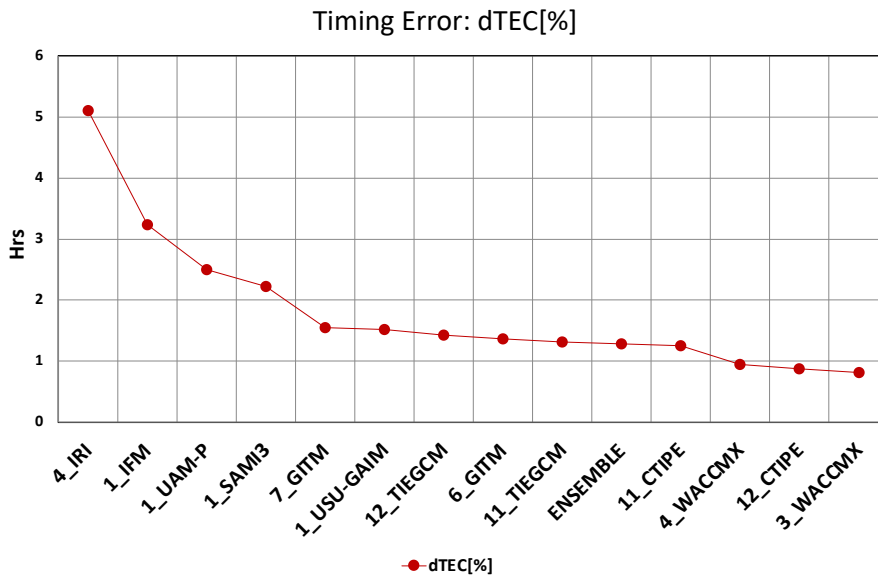
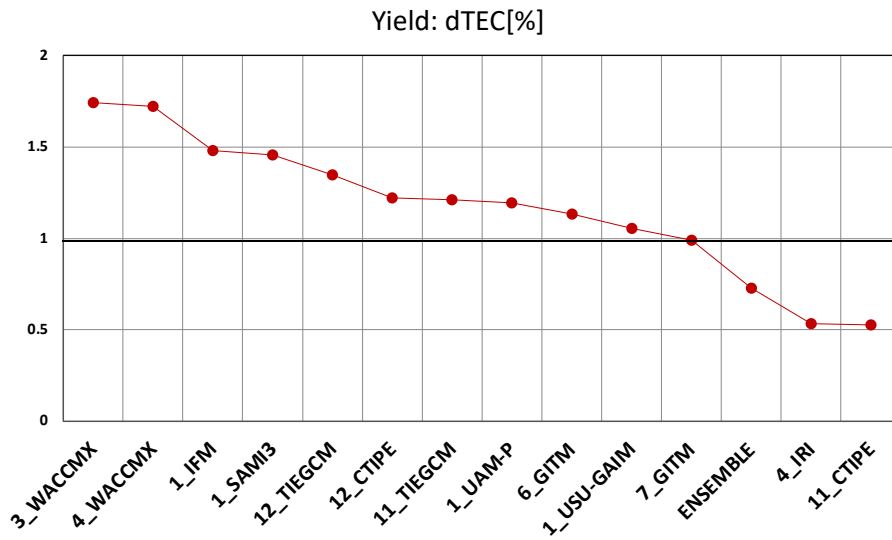


Figure 8

17 Figure 1. Scatter plots of the observed (x axis) and modeled (y axis) shifted foF2 and TEC (foF2*
18 in the 1st, TEC* in the 3rd columns), and percentage change of foF2 and TEC (dfoF2[%] in the
19 2nd, dTEC[%] in the 4th columns) during the storm (03/17/2013) for all 12 locations grouped into
20 North America (NA, green), Europe (EU, blue), South Africa (SAF, red), and South America
21 (SAM, black)

22

23 Figure 2. Correlation Coefficients (CC) between modeled and observed foF2 (left panel) and
24 TEC (right panel). Four CCs are displayed for each simulation: CC averaged over Europe (EU),
25 North America (NA), Southern Hemisphere (SH refers to SAF and SAM combined), and all 12
26 locations, from left to right. Different colors denote different quantities. Blue denotes shifted
27 foF2 and TEC, green and red the change and percentage changes, and black normalized
28 percentage change. The closer the circles are to the horizontal line of 1, the better the model
29 performances are.

30

31 Figure 3. Same as Figure 2 but for RMSE of shifted foF2 and TEC, and changes of foF2 and
32 TEC

33

34 Figure 4. Same as Figure 2 but for RMSE of percentage change of foF2 and TEC, and
35 normalized percentage change. Blue denotes dfoF2[%], red and black dTEC[%] and
36 dTEC[%]_norm.

37

38 Figure 5. Same as Figure 2 but for Yield (ratio) and absolute of Timing Error ($|TE| =$
39 $|t_{\text{peak_model}} - t_{\text{peak_obs}}|$)

40

41 Figure 6. Same as Figure 1 but for only TEC and dTEC[%] from the ensemble of the simulations
42 (ENSEMBLE) and 1_USU-GAIM

43

44 Figure 7. Averaged CC (a) and RMSE (b) over all 12 locations of 13 simulations, the ensemble
45 of them (ENSEMBLE), and the ensemble of 12 simulations excluding 1_USU-GAIM

46 (ENSEMBLE_wo_DA). Blue denotes shifted TEC, green and red the change and percentage

47 changes of TEC. CCs are plotted from the smallest to the largest (closer to 1) according to the

48 average of the three averaged CC values of TEC, dTEC and dTEC[%]. RMSEs are plotted from

49 the largest to the smallest according to the average RMSE for TEC and dTEC.

50

51 Figure 8. Yield and Timing Error of dTEC[%] for all 13 simulations and ENSEMBLE.

52

1 Table 1. Quantities and Skill Scores for Model-Data Comparison

| Quantities and skill scores for model-data comparison | |
|---|--|
| Quiet time references | 30-day median value at a given time: TEC_quiet(UT), 30 days consist of 15 days before (03/01-03/15/2013) and 15 days after (03/22-04/05/2013) the storm |
| Shifted TEC/foF2: | e.g., TEC*(doy, UT) = TEC(doy, UT) – minimum of TEC_quiet(UT) |
| TEC/foF2 changes w.r.t. the quiet time | e.g., dTEC(doy, UT) = TEC(doy, UT) – TEC_quiet(UT) |
| TEC/foF2 percentage changes w.r.t. the quiet time | e.g., dTEC[%](doy, UT) = 100 * dTEC(doy, UT) / TEC_quiet(UT) |
| Normalized Percentage changes of TEC | dTEC[%]_norm = (dTEC[%] - ave_dTEC[%]) / std_dTEC[%]; ave_dTEC[%] is the average of dTEC[%] at a given time and at a given location over the quiet 30 days, std_dTEC[%] is the standard deviation of the average percentage change |
| Skill Scores | |
| CC | Correlation Coefficient |
| RMSE | Root-Mean-Square Error ($= \sqrt{\frac{\sum(x_{obs} - x_{mod})^2}{N}}$), where x_{obs} and x_{mod} are observed and modeled values |
| Yield | ratio of the peak of modeled percentage change to that of the observed one ($= \frac{(x_{mod})_{max}}{(x_{obs})_{max}}$) |
| Timing Error (TE) | difference between the modeled peak time and observed peak time: TE = t_peak_model – t_peak_obs |

2

3

4

5

6

7 Table 2. Models used for this study

| Model Setting ID | Model Version | Drivers | | Upper boundary for TEC calculation/ Resolution |
|---|---|--|---|--|
| | | Input data | Models used for thermosphere, tides from lower boundary, and high latitude electrodynamics | |
| Physics-based Coupled Ionosphere-Thermosphere Model | | | | |
| | | | Tides | High Latitude Electrodynamics |
| 11_CTIPE ^a | CTIPe3.2 [<i>Codrescu et al.</i> , 2000; <i>Milward et al.</i> , 2001] | F10.7, ACE IMF data and solar wind speed and density, NOAA POES Hemispheric Power data | (2,2), (2,3), (2,4), (2,5), and (1,1) propagating tidal modes | Weimer-2005 high latitude electric potential [<i>Weimer</i> , 2005], Fuller-Rowell and Evans auroral precipitation [1987] |
| 12_CTIPE ^a | CTIPe4.1 | | WAM [<i>Akmaev et al.</i> , 2011, <i>Fuller-Rowell et al.</i> , 2010] tides | |
| 6_GITM ^a | GITM2.5 [<i>Ridley et al.</i> , 2006] | FISM solar EUV irradiance, ACE IMF data and solar wind speed and density | MSIS [<i>Hedin</i> , 1991] migrating diurnal and semidiurnal tides | Weimer-2005 high latitude electric potential, Ovation auroral precipitation [<i>Newell et al.</i> , 2009; 2011] |
| 7_GITM | GITM21.11 | | | Weimer-2005 high latitude electric potential, Fang's auroral precipitation [<i>Fang et al.</i> , 2013] |
| 12_TIE-GCM ^a | TIE-GCM2.0 [<i>Roble et al.</i> , 1988; <i>Richmond et al.</i> , 1992; <i>Solomon et al.</i> , 2012] | F10.7, Kp, OMNI IMF data and solar wind speed and density | GSWM [<i>Hagan et al.</i> , 1999] migrating diurnal and semidiurnal tides | Weimer-2005 high latitude electric potential, Roble and Ridley auroral precipitation [1987] |
| Whole Atmosphere Model | | | | |
| 3_WACCM-X | CESM2.2 [<i>Gottelman et al.</i> , 2019; <i>Liu et al.</i> , 2018] | F10.7, Kp, OMNI IMF data and solar wind speed and density | Heelis high latitude electric potential [<i>Heelis et al.</i> , 1982], Roble and Ridley auroral precipitation [1987] | ~600 km, 1.9° lat. × 2.5° long. |
| 4_WACCM-X | | | Weimer-2005 high latitude electric potential, Roble and Ridley auroral precipitation [1987] | |

8 ^aThe model results are submitted by the CCMC using the models hosted at the CCMC

10 Table 3. Number of locations where the models correctly predict negative or positive phase.

| | Time Interval | 11_CTIPE | 12_CTIPE | 6_GITM | 7_GITM | 12_TIE-GCM | 3_WACCM-X | 4_WACCM-X |
|----------|---------------|-----------|-----------|-----------|-----------|------------|-----------|-----------|
| dfoF2[%] | 06–15UT | 8 | 7 | 5 | 9 | 9 | 6 | 10 |
| | 15–22UT | 10 | 6 | 7 | 8 | 7 | 7 | 10 |
| dTEC[%] | 06–15UT | 9 | 10 | 10 | 10 | 7 | 10 | 9 |
| | 15–22UT | 7 | 10 | 12 | 11 | 10 | 7 | 8 |

11

12 Table 4. Averaged RMSE over all 12 locations of the ensemble of newer versions (ENSEMBLE_new) of models (12_CTIPE, 7_GITM and
 13 4_WACCM-X) driven by Weimer2005 electric potential model, the ensemble of older versions (ENSEMBLE_old) of models (11_CTIPE,
 14 6_GITM and 12_TIE-GCM), and 1_USU-GAIM.

| | TEC (TECU) | dTEC (TECU) | dTEC[%] |
|--------------|------------|-------------|---------|
| ENSEMBLE_old | 6.6 | 4.1 | 33.4 |
| ENSEMBLE_new | 4.6 | 3.2 | 29.8 |
| 1_USU-GAIM | 4.5 | 3.4 | 29.9 |

15

16

23 **Key Points:**

- 24 • foF2/TEC and their changes during a storm predicted by seven ionosphere-thermosphere
25 coupled models are evaluated against GIRO foF2 and GPS TEC measurements.
- 26 • Model simulations tend to underestimate the storm-time enhancements of foF2 and TEC
27 and to predict them better in the North America but worse in the southern hemisphere.
- 28 • Ensemble of all simulations for TEC is comparable to the data assimilation model (USU-
29 GAIM).
- 30

31 Abstract

32 Assessing space weather modeling capability is a key element in improving existing models and
33 developing new ones. In order to track improvement of the models and investigate impacts of
34 forcing, from the lower atmosphere below and from the magnetosphere above, on the
35 performance of ionosphere-thermosphere models, we expand our previous assessment for 2013
36 March storm event [*Shim et al.*, 2018]. In this study, we evaluate new simulations from upgraded
37 models (Coupled Thermosphere Ionosphere Plasmasphere Electrodynamics (CTIPE) model
38 version 4.1 and Global Ionosphere Thermosphere Model (GITM) version 21.11) and from
39 NCAR Whole Atmosphere Community Climate Model with thermosphere and ionosphere
40 extension (WACCM-X) version 2.2 including 8 simulations in the previous study. A simulation
41 of NCAR Thermosphere-Ionosphere-Electrodynamics General Circulation Model version 2
42 (TIE-GCM 2) is also included for comparison with WACCM-X. TEC and foF2 changes from
43 quiet-time background are considered to evaluate the model performance on the storm impacts.
44 For evaluation, we employ 4 skill scores: Correlation coefficient (CC), root-mean square error
45 (RMSE), ratio of the modeled to observed maximum percentage changes (Yield), and timing
46 error(TE). It is found that the models tend to underestimate the storm-time enhancements of foF2
47 (F2-layer critical frequency) and TEC (Total Electron Content) and to predict foF2 and/or TEC
48 better in the North America but worse in the Southern Hemisphere. The ensemble simulation for
49 TEC is comparable to results from a data assimilation model (Utah State University-Global
50 Assimilation of Ionospheric Measurement (USU-GAIM)) with differences in skill score less than
51 3% and 6% for CC and RMSE, respectively.

52

53 Plain Language Summary

54 The Earth's ionosphere-thermosphere (IT) system, which is present between the lower
55 atmosphere and the magnetosphere, is highly variable due to external forcings from below and
56 above as well as internal forcings mainly associated with ion-neutral coupling processes. The
57 variabilities of the IT system can adversely affect our daily lives, therefore, there is a need for
58 both accurate and reliable weather forecasts to mitigate harmful effects of space weather events.
59 In order to track the improvement of predictive capabilities of space weather models for the IT
60 system, and to investigate the impacts of the forcings on the performance of IT models, we
61 evaluate new simulations from upgraded models (CTIPe model version 4.1 and GITM version
62 21.11) and from NCAR WACCM-X version 2.2 together with 8 simulations in the previous
63 study. A simulation of NCAR TIE-GCM version 2 is also included for the comparison with
64 WACCM-X. Quantitative evaluation is performed by using 4 skill scores including Correlation
65 coefficient (CC), root-mean square error (RMSE), ratio of the modeled to observed maximum
66 percentage changes (Yield), and timing error (TE). The findings of this study will provide a
67 baseline for future validation studies of new and improved models.

68

69 **1. Introduction**

70 Variabilities of the Earth's ionosphere-thermosphere (IT) system, caused by charged
71 particles and electromagnetic radiation emitted from the sun, can adversely affect our daily lives,
72 which are highly dependent on space-based technological infrastructures such as Low-Earth
73 Orbit (LEO) satellites and the Global Navigation Satellite System (GNSS). To mitigate harmful
74 effects of space weather events, modeling plays a critical role in our quest to understand the
75 connection between solar eruptive phenomena and their impacts in interplanetary space and near-
76 Earth space environment. In particular, the Earth's upper atmosphere including the IT system is

77 the space environment closest to the human society. Thus, during the past few decades, first-
78 principles physics-based (PB) IT models have been developed for specifications and forecasts of
79 the near-Earth space environment. In addition, there have been recent developments of whole
80 atmosphere models with thermospheric and ionospheric extension to fully understand
81 variabilities of the IT system by considering coupling between the IT system and the lower
82 atmosphere [e.g., *Akmaev*, 2011; *Fuller-Rowell et al.*, 2010; *Jin et al.*, 2011; *Liu et al.*, 2018].

83 For more accurate space weather forecasting, assessing space weather modeling capability is
84 a key element to improve existing models and to develop new models. Over the last decade, in
85 an effort to address the needs and challenges of the assessment of our current knowledge about
86 space weather effects on the IT system and current state of IT modeling capabilities, the NASA
87 GSFC Community Coordinated Modeling Center (CCMC) has been supporting community-wide
88 model validation projects, including Coupling, Energetics and Dynamics of Atmospheric
89 Regions (CEDAR) [*Shim et al.*, 2011, 2012, 2014] and Geospace Environment Modeling
90 (GEM)-CEDAR modeling challenges [*Rastätter et al.*, 2016; *Shim et al.*, 2017a].

91 Furthermore, in 2018, the CCMC established an international effort, “International Forum
92 for Space Weather Modeling Capabilities Assessment”, to evaluate and assess the predictive
93 capabilities of space weather models (<https://ccmc.gsfc.nasa.gov/iswat/IFSWCA/>). As a result of
94 this international effort, four ionosphere/thermosphere working groups were established with an
95 overarching goal to devise a standardized quantitative validation procedure for IT models
96 [*Scherliess et al.*, 2019].

97 The working group, focusing on neutral density and orbit determination at LEO, reported
98 their initial results for specific metrics for thermosphere model assessment over the selected
99 three full years and two geomagnetic storms in 2005 [*Bruinsma et al.*, 2018]. They reported that

100 the tested models in general performed reasonably well, although seasonal errors were
101 sometimes observed and impulsive geomagnetic events remain a challenge. Kalafatoglu Eyigüler
102 et al. (2019) compared the neutral density estimates from two empirical and three PB models
103 with those obtained from the CHAMP satellite. They suggested that several metrics that provide
104 different aspects of the errors should be considered together for a proper performance evaluation.

105 Another working group, “Ionosphere Plasmasphere Density Working Team”, performed the
106 assessment of present modeling capabilities in predicting the ionospheric climatology of f_0F_2
107 and hmF_2 for the entire year 2012 [Tsaygouri et al., 2018]. Tsaygouri et al. (2018) identified a
108 strong seasonal and local time dependence of the model performances, especially for PB models,
109 which could provide useful insight for future model improvements. Tsaygouri et al. cautioned that
110 the quality of the ground truth data may play a key role in testing the model performance. Shim
111 et al. (2018) assessed how well the ionospheric models predict storm time f_0F_2 and TEC by
112 considering quantities, such as TEC and f_0F_2 changes and percentage changes compared to quiet
113 time background, at 12 selected midlatitude locations in the American and European-African
114 longitude sectors. They found that the performance of the model varies with locations, even
115 within a localized region like Europe, as well as with the metrics considered.

116 In this paper, we expand our previous assessment of modeled f_0F_2 and TEC during 2013
117 March storm event (17 March, 2013) [Shim et al., 2018] to track improvement of the models and
118 to investigate impacts of forcings from the lower atmosphere below and from the magnetosphere
119 above on the performance of IT models. For this study, we evaluate the updated version of the
120 coupled IT models available at the CCMC [Webb et al., 2009] since our previous study [Shim et
121 al., 2018]: CTIPe version 4.1 and GITM version 21.11. However, the other types of models such
122 as empirical models, stand-alone ionospheric models, and data assimilation models are not

123 included. In addition, for the first time, simulations of NCAR WACCM-X 2.2 are included in
124 our assessment. We also included a simulation of NCAR TIE-GCM 2 to compare with results
125 from WACCM-X 2.2. For TEC prediction, we compare a weighted mean of the ensemble of all
126 13 simulations (ensemble average), including 8 simulations from our previous study with
127 individual simulations to assess ensemble forecast capability. In Section 2, we briefly describe
128 observations, models, and metrics used for this study. Section 3 presents the results of model-
129 data comparisons and performance of the models are presented. Section 4 shows comparisons of
130 ensemble of TEC predictions with the individual simulations based on the skill scores used in
131 this study. Finally, we summarize and conclude in Section 5.

132

133 **2. Methodology**

134 **2.1 Observations and Metrics**

135 We use the foF2 and TEC measurements at 12 ionosonde stations selected in middle
136 latitudes: 8 northern hemisphere (NH) stations in the US (Millstone Hill, Idaho national Lab,
137 Boulder, and Eglin AFB) and Europe (Chilton, Pruhonice, Ebre, and Athens) and 4 southern
138 hemisphere (SH) stations in South America (Port Stanley) and South Africa (Louisvale,
139 Hermanus, and Grahamstown) (Figure 1 and Table 1 in *Shim et al.* [2018] for details). The foF2
140 and GNSS vertical TEC (vTEC) data are provided by Global Ionosphere Radio Observatory
141 (GIRO) (<http://giro.uml.edu/>) [*Reinisch and Galkin*, 2011] and by MIT Haystack Observatory
142 (<http://cedar.openmadrigal.org/>, <http://cedar.openmadrigal.org/cgi-bin/gSimpleUIAccessData.py>)
143 [*Rideout and Coster*, 2006], respectively.

144 Table 1 shows the quantities and skill scores calculated for model-data comparison. To
145 remove potential systematic uncertainties in the models and observations and baseline

146 differences among the models and between models and observations, we use the shifted values
147 and changes from their own quiet-time background values (e.g., shifted TEC (TEC^*) = TEC
148 (UT) on a particular DOY – median (UT) of TEC for 30 days centered on the storm date).
149 Furthermore, using these quantities likely reduce the impacts of differing upper boundaries for
150 TEC calculations, since the plasmaspheric TEC variations with geomagnetic activity are
151 negligible in middle latitudes [*Shim et al.*, 2017b].

152 To measure how well the observed and modeled values are linearly correlated (in phase)
153 with each other and how different the values are on average over the time interval considered,
154 CC and RMSE are calculated, respectively, for the error values below 95th percentile. We also
155 calculate Yield and timing error to measure the models' capability to capture peak disturbances
156 during the storm. For more detailed information on the quantities and skill scores used for the
157 study, refer to Section 2 in *Shim et al.* [2018].

158

159 **2.2 Models and Simulations**

160 The simulations used in this study are obtained from the updated and newly incorporated
161 coupled ionosphere-thermosphere models available at the CCMC [*Webb et al.*, 2009] since our
162 previous study [*Shim et al.*, 2018]: CTIPe 4.1, GITM 21.11 and WACCM-X 2.2. The WACCM-
163 X 2.2 simulations are provided by NCAR HAO. The WACCM-X version 2 [*Liu et al.*, 2018] is a
164 comprehensive numerical model that extends the atmospheric component model of the NCAR
165 Community Earth System Model (CESM) [*Hurrell et al.*, 2013] into the thermosphere up to
166 500–700 km altitude. WACCM-X is uniquely capable of being run in a configuration where the
167 atmosphere is coupled to active or prescribed ocean, sea ice, and land components, enabling
168 studies of thermospheric and ionospheric weather and climate. WACCM-X version 2 is based

169 upon WACCM version 6 [Gettelman *et al.*, 2019] with a top boundary of ~130 km, which is
170 built upon the Community Atmosphere Model (CAM) version 6 having a top boundary of ~40
171 km. WACCM-X 2.2 includes WACCM6 physics for middle atmosphere and lower thermosphere
172 as well as CAM6 physics for the troposphere and the lower stratosphere, and it fully incorporates
173 the electrodynamical processes related to low-to mid-latitude wind dynamo that is implemented
174 in the NCAR TIE-GCM. For this study, two specified-dynamics (SD) WACCM-X 2.2
175 simulations with different high-latitude electrostatic potential models [Heelis *et al.*, 1982;
176 Weimer, 2005] are used. The SD simulations are carried out by constraining the model's lower
177 atmospheric neutral dynamics using meteorological reanalysis data. The constraining process is
178 achieved by nudging the model towards MERRA-2 (Modern Era Retrospective Analysis for
179 Research and Applications, Version 2) data [Gelaro *et al.*, 2017] below around the altitude of 50
180 km in a way presented by Brakebusch *et al.* [2013].

181 The resulting WACCM-X simulations are compared with the simulations of TIE-GCM. The
182 comparisons between WACCM-X and TIE-GCM simulations will show differences and
183 similarities in modeling capabilities between whole atmosphere modeling and ionosphere-
184 thermosphere modeling with a specified low-boundary forcing (e.g., Global Scale Wave Model
185 (GSWM) [Hagan *et al.*, 1999] used for this study).

186 Table 2 shows the version of the models, input data used for the simulations, and models
187 used for lower boundary forcing and high latitude electrodynamics. We utilized unique model
188 setting identifiers to distinguish the current simulations from those used in our previous studies
189 [Shim *et al.*, 2011, 2012, 2014, 2017a, 2018]. Additional information for the models and model
190 setting identifiers is available in Shim *et al.* [2011] (Refer to all references therein) and at
191 https://ccmc.gsfc.nasa.gov/support/GEM_metrics_08/tags_list.php

192 To investigate improvement in foF2 and TEC predictions of the updated versions of CTIPE
193 (12_CTIPE) and GITM (7_GITM), the simulations of the old versions of the models (11_CTIPE
194 and 6_GITM) from our previous study are included. The comparison will be focused on the
195 comparison between the simulations obtained from the same model. As for TIE-GCM, 12_TIE-
196 GCM (run at 2.5° resolution) is presented for this study, but the comparison between
197 11_TIE_GCM and 12_TIE-GCM was not included in this study because the only difference
198 between the two is horizontal resolution (5°lat.×5°long. vs 2.5°lat.×2.5°long.).

199 We should take note of the difference between the simulations obtained from the same
200 model that influence foF2 and TEC responses to geomagnetic storms. For two CTIPE runs,
201 different lower atmospheric tides were specified: 11_CTIPE was driven by the imposed
202 migrating semidiurnal (2,2), (2,3), (2,4), (2,5), and diurnal (1,1) tidal modes, while 12_CTIPE
203 was run with monthly mean spectrum of tides obtained from WAM (Whole Atmosphere Model)
204 [Akmaev *et al.*, 2011, Fuller-Rowell *et al.*, 2010]. For two GITM simulations, 7_GITM used
205 Fang's auroral precipitation [Fang *et al.*, 2013], while 6_GITM used Ovation model [Newell *et*
206 *al.*, 2009; 2011]. For two WACCM-X simulations, Heelis and Weimer2005 electric potential
207 models were used for 3_WACCM-X and 4_WACCM-X, respectively. 12_TIEGCM was driven
208 by Weimer2005 electric potential model and GSWM.

209

210 **3. Performance of the Models in Predictions of foF2 and vTEC on 17 March 2013**

211 Most simulations newly added for this study show similar behavior to those used in Shim *et*
212 *al.* [2018], in predicting foF2 and TEC during the storm. For example, the simulations are not
213 able to reproduce (1) the difference between eastern and western parts of the North American
214 sector (e.g., TEC increases at Millstone Hill but decreases at Idaho and Boulder around 20UT),

215 and (2) different responses between foF2 (negligible changes) and TEC (noticeable increase)
216 found in European (Chilton) and South-African (Grahamstown) stations (See Figure 4 of Shim et
217 al. [2018] for reference). However, compared to other simulations, 4_WACCM-X driven by
218 *Weimer* (2005) high latitude electric potential model captures relatively well the two differences
219 in TEC and foF2 described above (Figure S1 in supporting information).

220 Figure 1 shows scatter plots of the observed (*x* axis) and modeled (*y* axis) shifted foF2 and
221 TEC, and percentage change of foF2 and TEC during the storm (03/17/2013) for all 12 locations
222 grouped into 4 sectors: North America (NA, green), Europe (EU, blue), South Africa (SAF, red),
223 and South America (SAM, black). First of all, the qualitative comparison between the
224 simulations from the same model can be summarized as follows. 11_CTIPE/12_CTIPE tends to
225 underestimate foF2 for both quiet and disturbed conditions, but 12_CTIPE predicts much better
226 both foF2 and TEC during the storm than 11_CTIPE. 6_GITM and 7_GITM underestimate foF2
227 and TEC for all cases and show relatively small response to the storm compared to the other
228 simulations. 12_TIE-GCM and WACCM-Xs produce similar foF2 and TEC changes during the
229 storm. All three simulations give *substantial underestimation of TEC in SAF*. 12_TIE-GCM and
230 3_WACCM-X produce larger overestimation of foF2 and TEC in NA sector than 4_WACCM-X.
231 4_WACCM-X shows substantial improvement in the TEC overestimation in NA. 3_WACCM-X,
232 of which the high latitude electric potential is specified by Heelis et al. [1982], tends to
233 overestimate foF2 and TEC compared with 4_WACCM-X. 3_WACCM-X and 4_WACCM-X
234 produce better quiet time foF2 and TEC than 12_TIEGCM does and capture wave-like small
235 increases in foF2 and TEC at Idaho National Lab around 10–11UT (2–3 LT) (Figure S1 in
236 supporting information).

237 As shown for 6_GITM and 11_CTIPE in *Shim et al.* [2018], the modeled foF2 values of
238 7_GITM and 12_CTIPE better agrees with the observed ones when they are shifted by
239 subtracting the minimum of 30-day median (see Figure S2 in supporting information, *Shim et al.*
240 [2018]). Most foF2 and TEC data points of 7_GITM and 12_CTIPE before shifting are below
241 and above the line with slope 1 (black solid line), respectively. This indicates that 7_GITM
242 underestimates foF2 and TEC like 6_GITM, while 12_CTIPE overestimates them. The models
243 that tend to underestimate foF2, such as 6_GITM, 7_GITM and 11_CTIPE, seem to unable to
244 produce foF2* larger than about 7 MHz, and underestimate TEC* being less than about 20
245 TECU during the storm as reported in *Shim et al.* [2018]. 12_TIE-GCM and WACCM-Xs show
246 similar distribution of the data points after shifting foF2 and TEC with a tendency to
247 underestimate foF2 and TEC in the South Africa region.

248 The modeled dfoF2[%] and dTEC[%] show less agreement with the observed values than
249 the modeled foF2* and TEC* do. The data points in the 2nd quadrant (top left) and the 4th
250 quadrant (bottom right) indicate that the modeled and observed percentage changes are in
251 opposite sign. 7_GITM and 3_WACCM-X have more data points in the 2nd quadrant for
252 dfoF2[%] prediction than 6_GITM and 4_WACCM-X, respectively. Like most simulations used
253 in our previous evaluation [*Shim et al.* 2018], 12_CTIPE and 7_GITM do not appear to
254 reproduce the large dTEC[%] (about 200 %) at Port Stanley in SAM. However, 12_TIE-GCM
255 and WACCM-Xs better produce the enhancement in TEC percentage change. Compared to
256 4_WACCM-X and 12_TIE-GCM, 3_WACCM-X overestimates dTEC[%] especially in NA and
257 EU regions. 12_CTIPE and 6_GITM have more data points of overestimated dTEC[%] in SAF
258 than 11_CTIPE and 7_GITM, respectively.

259 From now on, foF2 and TEC will represent shifted foF2 (foF2*) and shifted TEC (TEC*),
260 respectively.

261

262 **3.1 Correlation Coefficient (CC)**

263 We first calculate correlation coefficient (CC) between the modeled and observed foF2 and
264 TEC for DOY 076 (17 March, 2013) for quantitative assessment of the model performance of
265 TEC and foF2 predictions. In Figure 2, the CCs for each simulation are presented for foF2 in the
266 left panel and for TEC in the right panel. For each simulation, four CC values are displayed. First
267 three of the values correspond to the average CC over Europe (EU), North America (NA),
268 Southern Hemisphere (SH refers to SAF and SAM combined), and the last one is the average of
269 all 12 locations. The modeled foF2 and TEC (blue dots) are highly correlated with the observed
270 values. The average CC values over all 12 locations for both foF2 and TEC are about 0.8–0.95,
271 but the average CCs for their changes are much smaller. For example, the CCs for TEC changes
272 (dTEC) are 0.5–0.6 and even smaller for foF2. The modeled foF2 changes (green), percentage
273 changes (red) and normalized percentage changes (black only applicable for TEC) are much less
274 correlated (closer to uncorrelated) with the observed values (about $0.1 < \text{average CC} < 0.4$).
275 There is no big difference between dTEC[%] and dTEC[%]_norm based on the average values
276 for each simulation as reported in *Shim et al.* [2018].

277 Note that the CC values for the changes and percentage changes of foF2 and TEC are highly
278 dependent on locations. Most simulations, except for 12_CTIPE and GITMs, show lower CC for
279 dfoF2 and dTEC in NA. It seems to be caused by the decreases of foF2 and TEC during the
280 storm (negative phase) in the western parts of NA that are not captured well. GITMs show the

281 negative phase well although it underestimated the magnitude of the change. The CCs for the
282 percentage changes of foF2 and TEC are particularly small for CTIPEs and GITMs.

283 11_CTIPe's foF2 and TEC averaged over 12 locations are slightly better correlated with the
284 observed values than 12_CTIPe. However, the changes and percentage changes of foF2 and
285 TEC from 12_CTIPe are better correlated with the observed values than 11_CTIPe's values in
286 most regions. Although the two GITMs produce similar CCs, 7_GITM shows better CC in NA
287 regions for dfoF2, dfoF2[%], dTEC[%], and n_dTEC[%], while 6_GITM shows better CC for
288 foF2 and dTEC. WACCM-Xs perform better than 12_TIE_GCM for all the considered quantities
289 based on the average except for dTEC. WACCM-Xs perform similar to each other.

290 Close inspection of Figures. 1 and 2 indicates that a linearity between CTIPe and
291 observations is improved in the newer version of CTIPe (12_CTIPe), but 12_CTIPe gives more
292 scattered distribution around a linear relation (Fig. 1), which seems to lead to the lower CC in
293 12_CTIPe than in 11_CTIPe. 7_GITM exhibits a slight improvement in a linearity between the
294 model and observations (Fig. 1), but this improvement is not clearly seen in the correlation
295 analysis (Fig. 2). For 12_TIEGCM and WACCM-Xs, both a linearity between the models and
296 observations (Fig. 1) and CCs (Fig. 2) demonstrate that the model performances are overall
297 improved in WACCM-Xs compared with TIEGCM. In terms of the model-observation linearity,
298 4_WACCMX is somewhat better than 3_WACCMX (Fig. 1), but their CCs seems comparable to
299 each other (Fig. 2).

300

301 **3.2 Root Mean Square Error (RMSE)**

302 Figure 3 shows RMSE of foF2 and dfoF2 in the left panel, and TEC and dTEC in the right
303 panel. For foF2 (blue) and dfoF2 (green) predictions, based on the average RMSE values, the

304 RMSEs from the updated version (12_CTIPE and 7_GITM) are about 1.5 MHz for foF2 and
305 about 1 MHz for dfoF2, and they are slightly lower than RMSEs in their old versions. 12_CTIPE
306 shows improvement in foF2 in SH and dfoF2 in NA and EU compared to 11_CTIPE. 7_GITM
307 performs better in foF2 and dfoF2 in EU and SH than 6_GITM. 4_WACCM-X has smaller
308 RMSE (~1 MHz) than 3_WACCM-X and 12_TIE-GCM (~1.3 MHz for dfoF2 and ~2 MHz for
309 foF2).

310 12_CTIPE is better in TEC prediction than 11_CTIPE, while the opposite holds true for
311 dTEC prediction. The two GITMs' average RMSE values for TEC and dTEC predictions are
312 similar to each other, about 9 TECU for TEC and 5 TECU for dTEC. Like foF2 and dfoF2
313 prediction, 4_WACCM-X has smaller RMSE (~ 5 TECU for TEC and 4 TECU for dTEC) than
314 12_TIE-GCM and 3_WACCM-X (~6 TECU).

315 As seen in *Shim et al.* [2018], RMSE is highly variable with location. Most simulations
316 appear to predict foF2 and/or TEC better in NA and worse in SH (except for 12_TIE-GCM for
317 foF2 and 12_CTIPE for TEC). Both 11_CTIPE and GITMs tend to perform better in NA for
318 dTEC, while WACCM-Xs show the opposite tendency for dfoF2 and dTEC. 7_GITM and
319 4_WACCM-X shows the least RMSE dependence on location for dfoF2 and for dTEC,
320 respectively, among seven simulations.

321 Figure 4 shows the RMSE of percentage changes of foF2 (blue) and TEC (red) and
322 normalized percentage changes of TEC (black). The two CTIPEs produce the similar RMSE for
323 dTEC[%], but 12_CTIPE and 11_CTIPE produce lower RMSE for dfoF2[%] and
324 dTEC[%]_norm, respectively. For all three percentage changes of dfoF2[%], dTEC[%], and
325 dTEC[%]_norm, 7_GITM seems to perform better than 6_GITM based on the average RMSEs

326 over the 12 locations. 4_WACCM-X and 12_TIE-GCM perform very similarly for dfoF2[%] and
327 dTEC[%] and better than 3_WACCM-X.

328 Difference in the performance among locations is more noticeable in dTEC[%] and
329 dTEC[%]_norm than in dfoF2[%] as found in *Shim et al.* [2018]. All simulations, except
330 6_GITM, produce lower RMSE of dTEC[%] in NA and higher in SH region. This tendency
331 remains the same for dTEC[%]_norm with the exception of 3_WACCM-X, which has lower
332 RMSE for dTEC[%]_norm in SH. For 3_WACCM-X, the higher RMSE for dTEC[%] and the
333 lower RMSE for dTEC[%]_norm in SH than in NA are probably due to the normalization factor,
334 standard deviation of dTEC[%] in the locations.

335

336 **3.3 Yield and Timing Error (TE)**

337 To measure how well the models capture the degree of TEC and foF2 disturbances during
338 the main phase, Yield and Timing Error (TE) of dfoF2[%], dTEC[%], and dTEC[%]_norm are
339 calculated. *Shim et al.* [2018] considered two time intervals, 06–15UT and 15–22UT, when
340 peaks are observed in most of 12 locations. In each time interval, we calculate one Yield value
341 and one TE value. Definitions of Yield and TE are presented in Table 1.

342 In each sector, average Yield and TE are calculated over the number of stations where the
343 model correctly predicts the storm phase, i.e., Yield is positive. Table 3 shows the total number
344 of stations where the models show correct storm phase, either positive or negative. The numbers
345 in bold are the higher values between the simulations compared. 12_CTIPE predicts the storm
346 phase better for dTEC[%] than 11_CTIPE, but 11_CTIPE predicts better for dfoF2[%] than
347 12_CTIPE. 7_GITM is improved in predicting the storm phase of dfoF2[%], while 6_GITM
348 predicts better the storm phase of dTEC[%]. 4_WACCM-X, compared to 12_TIE-GCM and

349 3_WACCM-X, is better for predicting the phase of dfoF2[%] and worse for predicting that of
 350 dTEC[%].

351 Figure 5 shows average Yield (left) and average of absolute values of TE (right) over the
 352 two time intervals: dfoF2[%] in blue, dTEC[%] in red, and dTEC[%]_norm in black. Concerning
 353 the average of all 12 locations, 12_CTIPE appears to overestimate peak values of dTEC[%] and
 354 dTEC[%]_norm with larger variation with location (e.g., $\sim 1 < \text{Yield of dTEC}[\%]_{\text{norm}} < \sim 2.5$)
 355 than 11_CTIPE, of which Yield is less than 1 for all three quantities of percentage changes (e.g.,
 356 $0.7 < \text{Yield of dTEC}[\%]_{\text{norm}} < 0.9$). Yields of 12_CTIPE for dTEC[%] and dTEC[%]_norm
 357 are closer to 1 in NA. GITMs produce similar ratios based on the average over all locations, but
 358 7_GITM shows smaller differences in Yield among locations (e.g., $\sim 0.5 < \text{Yield of}$
 359 $\text{dTEC}[\%]_{\text{norm}} < \sim 1$) than 6_GITM (e.g., $0.5 < \text{Yield of dTEC}[\%]_{\text{norm}} < \sim 2.5$). In terms of
 360 average Yield, 12 TIE-GCM and two WACCM-Xs tend to overestimate the peak values and
 361 show similar performance, although 12_TIE-GCM's ratios are closer to 1 than those of
 362 WACCM-Xs. 3_WACCM-X shows larger variation in Yield among locations (e.g., $\sim 0.9 < \text{Yield}$
 363 $\text{of dTEC}[\%]_{\text{norm}} < \sim 2.7$) than 12_TIE-GCM and 4_WACCM-X (e.g., $\sim 1.7 < \text{Yield of}$
 364 $\text{dTEC}[\%]_{\text{norm}} < \sim 2.3$).

365 Average Timing Errors of dfoF2[%] and dTEC[%]_norm are between 1 and 2 hours, and
 366 TE of dTEC[%] are about 0.8–1.5 hours. With respect to the average TE, 12_CTIPE has smaller
 367 TE (~ 1 hr) than 11_CTIPE (about 1.5 hr) for all three percentage changes with less location
 368 dependence as well. 7_GITM's three TEs are about 1.5 hrs, while 6_GITM's TEs of dfoF2[%],
 369 dTEC[%] and dTEC[%]_norm are ~ 1 , ~ 1.4 , and ~ 2 hrs, respectively. 12 TIE-GCM has smaller
 370 TE for dfoF2[%] and 3_WACCM-X has smaller TE for dTEC[%] and dTEC[%]_norm, however
 371 3_WACCM-X show larger location dependence of TE for dTEC[%]_norm and dfoF2[%].

372

373 **4. Ensemble of TEC obtained from 13 simulations**

374 The linearity check, RMSE, and CC between model results and observations for shifted foF2
375 and TEC and their relative changes indicate that the newer versions of the models (i.e.,
376 12_CTIPE, 7_GITM and 4_WACCM-X) produces the better results. From the viewpoints of
377 correct prediction of storm phases (Table 3), Yields, and TEs (Fig. 5), however, there is no one
378 best simulation for all locations, and the performance of model varies with locations as well as
379 the Yields and TE.

380 The differences in performance among the simulations could be caused by inherent
381 differences among the models or by a combination of different input data and different models
382 used for lower boundary forcing and high-latitude electrodynamics. Even different data
383 assimilation models for the same weather condition can yield different results, due to numerous
384 reasons (e.g., the use of different background weather models, spatial/temporal resolutions,
385 assimilation methods, and data error analyses), even if the same data are assimilated [*Schunk et*
386 *al.*, 2021]. The common way to handle these differences is to use model ensembles and the use
387 of ensembles enables estimations of the certainty of results. Thus, we used a weighted mean of
388 the ensemble of all 13 simulations including 8 simulations from our previous study (*Shim et al.*,
389 2018) for TEC, dTEC and dTEC[%] to compare the ensemble average with the individual
390 simulations. To get the weighted mean ($\bar{x} = \sum w_i x_i / \sum w_i$), we used the RMSE of shifted TEC
391 ($w_i = 1/\text{RMSE}$).

392 Figure 6 is the same as Figure 1 but for the ensemble of the simulations (ENSEMBLE will
393 be used as model setting ID) and a simulation (1_USU-GAIM) from a data assimilation model
394 (DA), USU-GAIM. For TEC less than about 20 TECU, ENSEMBLE shows better agreement

395 with GPS TEC than the individual simulations, including 1_USU-GAIM. However, as we can
396 expect, ENSEMBLE underestimates TEC larger than about 30 TECU due to the tendency to
397 underestimate TEC of many simulations as pointed out in Section 3 and *Shim et al.*, [2018]. For
398 dTEC[%], ENSEMBLE appears to be correlated better with GPS dTEC[%] than the other
399 simulations, although there are some underestimations in SAF, as well as in SAM with opposite
400 prediction of the storm phase.

401 Figure 7 shows averaged CC and RMSE values over all 12 locations of 13 simulations, the
402 ensemble of them, and the ensemble of 12 simulations excluding 1_USU-GAIM
403 (ENSEMBLE_wo_DA). The simulations in Figure 7 (a) were arranged by the average of the
404 three averaged CC values for TEC, dTEC and dTEC[%] from the smallest to the largest (closer
405 to 1). In Figure 7 (b), the simulations were arranged by the average of the two averaged RMSEs
406 for TEC and dTEC from the largest to the smallest. Based on the averaged CC and RMSE,
407 ENSEMBLES (ENSEMBLE and ENSEMBLE_wo_DA) of the simulations perform very
408 similarly and outperform all 12 simulations but a data assimilation model, 1_USU-GAIM.
409 However, ENSEMBLES and 1_USU-GAIM do not show big difference in their performance.
410 The differences in RMSE of TEC and dTEC between ENSEMBLE and 1_USU-GAIM are less
411 than 0.5 and 0.1 TECU, respectively. For dTEC[%], ENSEMBLE performs slightly better than
412 1_USU-GAIM with about 1.5% lower RMSE. The fact that ENSEMBLES are comparable to the
413 data assimilation model 1_USU-GAIM indicates that the multi-model ensemble can be useful in
414 forecasting the IT system, although this result is obtained from a single geomagnetic storm event.

415 Figure 8 shows Yield and Timing Error of dTEC[%] for all 13 simulations along with
416 ENSEMBLE. The values correspond to the average over all 12 locations. Unlike CC and RMSE,
417 ENSEMBLE does not outperform all physic-based coupled models in terms of Yield and TE,

418 although the difference is small. ENSEMBLE underestimates Yield, while most of the
419 simulations overestimate it, except 4_IRI and 11_CTIPE. 7 simulations from PB coupled IT
420 models and 1_USU-GAIM produce Yield closer to 1 than ENSEMBLE does.

421 Timing Error of dTEC[%] of ENSEMBLE is about 1 hr, which is slightly larger than TE
422 from 4 simulations from CTIPE and WACCM-X, but the difference from the smallest TE is less
423 than 0.5 hr.

424 Regarding the averaged skill scores for all 12 locations, newly added five simulations in this
425 study produce comparable TEC and TEC changes to the simulations from PB IT models used in
426 our previous study. The simulations of newer versions of the models (12_CTIPE, 7_GITM and
427 4_WACCM-X) are found to give overall improved forecast results. Based on the averaged
428 RMSE, the ensemble of simulations of the models' newer versions is comparable to 1_USU-
429 GAIM and performs better than the ensemble of the simulations of old versions of models
430 (11_CTIPE, 6_GITM and 12_TIE-GCM) (Table 4).

431

432 **5. Summary and Conclusions**

433 We expanded on our previous systematic assessment of modeled foF2 and TEC during
434 2013 March storm event (17 March, 2013) to track the improvement of the models and
435 investigate impacts of forcings from the lower atmosphere and the magnetosphere, on the
436 performance of ionosphere-thermosphere coupled models.

437 We evaluated simulations from upgraded models (CTIPE4.1 and GITM21.11) since our
438 previous assessment and a whole atmosphere model (WACCM-X2.2). To compare with results
439 from WACCM-X2.2, we also included a simulation of TIE-GCM2.0, of which the
440 electrodynamic processes are implemented in WACCM-X 2.2. Furthermore, to evaluate TEC

441 prediction of the simulations, we used a weighted mean of the ensemble of all 13 simulations
442 including 8 simulations from our previous study to compare the ensemble average with the
443 individual simulations.

444 For evaluation of the simulations, we used the exact same procedure with the same data set,
445 same physical quantities, and same skill scores as our previous study [*Shim et al.*, 2018]. The
446 skill scores were calculated for the three sectors, EU (Europe), NA (North America), and SH
447 (Southern Hemisphere) to investigate the longitudinal and hemispheric dependence of the
448 performance of the models.

449 From the five simulations used in the study, we also found the general behaviors of most
450 simulations identified in *Shim et al.* [2018]: 1) tendency to underestimate storm-time
451 enhancements of foF2 and TEC and not to reproduce large enhancements of dTEC[%] (e.g.,
452 about 200 % TEC increase at Port Stanley in the SAA region), 2) being unable to capture
453 opposite responses to the storm in the eastern and western parts of NA, especially negative phase
454 (except for GITM), which is what in part causes lower CC in NA, 3) tendency to predict foF2
455 and/or TEC better in NA and worse in SH with respect to RMSE. However, it was found that
456 12_TIE-GCM and WACCM-Xs better produce the large TEC percentage changes at Port Stanley
457 in SAM. Based on the averaged skill scores for all 12 locations, the five simulations used in this
458 study show skill scores better or comparable to those of the simulations from PB IT models used
459 in our previous study.

460 Compared to 11_CTIPE (obtained from CTIPe3.2), 12_CTIPE (from CTIPe4.1) driven by
461 tides from WAM tends to overestimate foF2 and TEC for both quiet and disturbed conditions
462 and predicts better TEC peaks during the storm. For more cases, 12_CTIPE performs largely
463 better than 11_CTIPE based on the average scores. 12_CTIPE predicts the storm phase better for

464 dTEC[%], but 11_CTIPE does better for dfoF2[%]. 12_CTIPE appears to overestimate peak
465 values of dTEC[%] and dTEC[%]_norm, while 11_CTIPE produces Yield less than 1.

466 The two GITMs, 7_GITM with Fang's auroral precipitation and 6_GITM with Ovation
467 model, underestimate foF2 and TEC for all cases and show relatively small response to the storm
468 compared to the other simulations that do not appear to reproduce the large dTEC[%] (about
469 200 % increase at Port Stanley in SAM). 7_GITM and 6_GITM perform very similarly for most
470 cases with similar skill scores. However, 7_GITM shows better CC for most quantities except for
471 dTEC, and lower RMSEs and Yield closer to 1 for most regions and quantities considered.
472 7_GITM shows the least RMSE dependence on location for dfoF2 among the other simulations.

473 Comparing two WACCM-Xs and 12_TIE-GCM, the two WACCM-Xs, 3_WACCM-X with
474 Heelis high latitude electric potential model and 4_WACCM-X with Weimer 2005, predict quiet
475 time foF2 and TEC better than 12_TIE-GCM. During the storm, 12_TIE-GCM and 4_WACCM-
476 X produce similar foF2 and TEC in NA sector, while 3_WACCM-X tends to overestimate them
477 and produces larger changes in foF2 and TEC. In most cases, WACCM-Xs and 12_TIE_GCM
478 perform similarly in terms of average values of skill scores, but 3_WACCM-X and/or
479 4_WACCM-X perform better than 12_TIE-GCM except for Yield of percentage changes.
480 4_WACCM-X slightly outperforms 3_WACCMX for all cases but not for TE for percentage
481 changes.

482 Our findings suggest that the newer versions of the models (12_CTIPE, 7_GITM and
483 4_WACCM-X) with Weimer2005 electric potential model give overall improved forecast, and
484 the performance of the models depends on forcing from the magnetosphere and also forcing from
485 the lower atmosphere even during storms.

486 For TEC, dTEC and dTEC[%], our results indicate that the ensemble of all 13 simulations
487 (ENSEMBLE), including 8 simulations from our previous study (*Shim et al.*, 2018) is
488 comparable to the data assimilation model (1_USU-GAIM) with differences in skill score less
489 than 3% and 6% for CC and RMSE, respectively. However, ENSEMBLE underestimates Yield
490 (0.73) while 7 simulations from PB coupled IT models and 1_USU-GAIM produce Yield closer
491 to 1. Timing Error of dTEC[%] of ENSEMBLE is about 1 hr, but the difference from the
492 smallest TE of the simulations is less than 0.5 hr. In addition, based on RMSE, the ensemble of
493 the newer versions of the models (12_CTIPE, 7_GITM and 4_WACCM-X) is comparable to
494 1_USU-GAIM.

495 To advance our understanding of the ionosphere-thermosphere system requires significant
496 efforts to improve the capability of numerical models along with the scope of observations
497 [*Heelis and Maute*, 2020]. There have been recent new developments of theoretical models,
498 including AMGeO (Assimilative Mapping of Geospace Observations) for High-Latitude
499 Ionospheric Electrodynamics [*Matsuo*, 2020] and MAGE geospace model that couples the Grid
500 Agnostic MHD for Extended Research Applications (GAMERA) global MHD model of
501 the magnetosphere (Sorathia et al., 2020; Zhang et al., 2019), the Rice Convec-tion Model
502 (RCM) model of the ring current (Toffoletto et al., 2003), TIEGCM of the upper atmosphere and
503 the RE-developed Magnetosphere-Ionosphere Coupler/Solver (REMIX) (Merkin & Lyon, 2010).
504 These models will be available soon to the public through CCMC, and then the modeling
505 capability will help us better understand the processes responsible for the observed
506 characteristics and features during disturbed conditions. In addition, CCMC will also provide
507 users with the capability to run PB IT models with various combination of models for lower

508 atmospheric forcing and for magnetosphere forcing, which enable us to research further the
509 impacts of the forcings on the IT system.

510 The findings of this study will provide a baseline for future validation studies using new
511 models and improved models, along with earlier results [*Shim et al.*, 2011, 2012, 2014, 2017a,
512 2018] obtained through CEDAR ETI, GEM-CEDAR Modeling Challenges, and the international
513 effort, “International Forum for Space Weather Modeling Capabilities Assessment”. We will
514 extend our study to include more geomagnetic storm events to investigate differences and
515 similarities in the performance of the models. In addition, we will also include foF2 and TEC
516 predictions for the high- and low-latitude regions.

517

518 **Acknowledgement**

519 This work was supported by Korea Polar Research Institute (KOPRI) grant funded by the
520 Ministry of Oceans and Fisheries (KOPRI PE22020) and basic research funding from the Korea
521 Astronomy and Space Science Institute (KASI) (KASI2022185009). The vertical TEC data were
522 provided by MIT Haystack Observatory and can be obtained through CEDAR Madrigal database
523 (<http://cedar.openmadrigal.org>). We thank the operators of the digisondes for sharing their data
524 through <http://giro.uml.edu/>. Data from the South African Ionosonde network is made available
525 through the South African National Space Agency (SANSA), who are acknowledged for
526 facilitating and coordinating the continued availability of data. This work is supported by grants
527 from the National Science Foundation (NSF) Space Weather Program. This model validation
528 study is supported by the Community Coordinated Modeling Center (CCMC) at the Goddard
529 Space Flight Center. Data processing and research at MIT Haystack Observatory are supported
530 by cooperative agreement AGS-1242204 between the U.S. National Science Foundation and the

531 Massachusetts Institute of Technology. The National Center for Atmospheric Research is
532 sponsored by the National Science Foundation. Model output and observational data used for the
533 study will be permanently posted at the CCMC website (<http://ccmc.gsfc.nasa.gov>) and provided
534 as a resource for the space science community to use in the future.

535

536

537 **References**

538 Akmaev, R. A. (2011). Whole atmosphere modeling: Connecting terrestrial and space weather.
539 *Reviews of Geophys.* 49, RG4004. 390 <https://doi.org/10.1029/2011RG000364>

540 Brakebusch, M., Randall, C. E., Kinnison, D. E., Tilmes, S., Santee, M. L., and Manney, G. L.
541 (2013) Evaluation of Whole Atmosphere Community Climate Model simulations of ozone
542 during Arctic winter 2004–2005, *J. Geophys. Res.*, 118, 2673–2688,
543 <https://doi.org/10.1002/jgrd.50226>

544 Bruinsma, S., Sutton, E., Solomon, S. C., Fuller-Rowell, T., & Fedrizzi, M. (2018). Space
545 weather modeling capabilities assessment: Neutral density for orbit determination at low Earth
546 orbit. *Space Weather*, 16, 1806–1816. <https://doi.org/10.1029/2018SW002027>

547

548 Chamberlin, P. C., Woods, T. N., & Eparvier, F. G. (2007). Flare Irradiance Spectral Model
549 (FISM): Daily component algorithms and results. *Space Weather*, 5, S07005.
550 <https://doi.org/10.1029/2007SW000316>

- 551 Codrescu, M. V., T. J. Fuller-Rowell, J. C. Foster, J. M. Holt, and S. J. Cariglia, (2000), Electric
552 field variability associated with the Millstone Hill electric field model, *J. Geophys. Res.*, 105,
553 5265–5273, doi:10.1029/1999JA900463.
- 554 Fang, X., D. Lummerzheim, and C. H. Jackman (2013), Proton impact ionization and a fast
555 calculation method, *J. Geophys. Res. Space Physics*, 118, 5369–5378, doi:10.1002/jgra.50484.
- 556 Fuller -Rowell, T. J., and D. S. Evans, (1987), Height-Integrated Pedersen and Hall Conductivity
557 Patterns Inferred From the TIROS-NOAA Satellite Data, *J. Geophys. Res.*, 92(A7), 7606–7618.
- 558 Fuller-Rowell, T., Wu, F., Akmaev, R., Fang, T.-W., & Araujo-Pradere, E. (2010). A whole
559 atmosphere model simulation of the impact of a sudden stratospheric warming on thermosphere
560 dynamics and electrodynamics. *Journal of Geophysical Research*, 115, A00G08. [https://](https://doi.org/10.1029/2010JA015524)
561 doi.org/10.1029/2010JA015524
- 562 Gelaro, R., McCarty, W., Suárez, M. J., Todling, R., Molod, A., Takacs, L., et al. (2017). The
563 Modern-Era Retrospective Analysis for Research and Applications, version 2 (MERRA-2).
564 *Journal of Climate*, 30(14), 5419–5454. <https://doi.org/10.1175/JCLI-D-16-0758.1>
- 565 Gettelman, A., Mills, M. J., Kinnison, D. E., Garcia, R. R., Smith, A. K., Marsh, D. R., et
566 al.(2019). The whole atmosphere community climate model version 6 (WACCM6), *Journal of*
567 *Geophysical Research: Atmospheres*, 124, 12,380–12,403. [https://doi.org/](https://doi.org/10.1029/2019JD030943)
568 [10.1029/2019JD030943](https://doi.org/10.1029/2019JD030943).
- 569 Hagan, M. E., M. D. Burrage, J. M. Forbes, J. Hackney, W. J. Randel, and X. Zhang, (1999),
570 GSWM-98: results for migrating solar tides. *J. Geophys. Res.* 104: 6813–6828.

- 571 Hedin, A. E. (1991), Extension of the MSIS thermospheric model into the middle and lower
572 atmosphere, *J. Geophys. Res.*, 96, 1159–1172.
- 573 Heelis, R. A., J. K. Lowell, and R. W. Spiro, (1982), A Model of the High-Latitude Ionospheric
574 Convection Pattern, *J. Geophys. Res.* 87, 6339.
- 575 Heelis, R. A., & Maute, A. (2020). Challenges to understanding the Earth's ionosphere and
576 thermosphere. *JGR: Space Physics*, 125, [https:// doi.org/10.1029/2019JA027497](https://doi.org/10.1029/2019JA027497)
- 577 Jin, H., Miyoshi, Y., Fujiwara, H., Shinagawa, H., Terada, K., Terada, N., et al. (2011). Vertical
578 connection from the tropospheric activities to the ionospheric longitudinal structure simulated by
579 a new Earth's whole atmosphere-ionosphere coupled model. *Journal of Geophysical Research*,
580 116, A01316. <https://doi.org/10.1029/2010JA015925>
- 581 Kalafatoglu Eyiguler, E. C., Shim, J. S., Kuznetsova, M. M., Kaymaz, Z., Bowman, B. R.,
582 Codrescu, M. V., et al. (2019). Quantifying the storm time thermospheric neutral density
583 variations using model and observations. *Space Weather*, 17, 269–284.
584 <https://doi.org/10.1029/2018SW002033>.
- 585 Liu, H.-L., Bardeen, C. G., Foster, B. T., Lauritzen, P., Liu, J., Lu, G., . . . Wang, W. (2018). Development
586 and validation of the Whole Atmosphere Community Climate Model with thermosphere and ionosphere
587 extension (WACCM-X 2.0), *Journal of Advances in Modeling Earth Systems*, 10. [https://doi.org/10.1002/](https://doi.org/10.1002/2017MS001232)
588 2017MS001232
- 589
- 590 Matsuo, T. (2020). Recent Progress on Inverse and Data Assimilation Procedure for High-
591 Latitude Ionospheric Electrodynamics. In: Dunlop, M., Lühr, H. (eds) *Ionospheric Multi-*

- 592 Spacecraft Analysis Tools. ISSI Scientific Report Series, vol 17. Springer, Cham.
593 https://doi.org/10.1007/978-3-030-26732-2_10
- 594 Merkin, V., & Lyon, J. (2010). Effects of the low-latitude ionospheric boundary condition on the
595 global magnetosphere. *Journal of Geophysical Research*, 115(A10). A10202.
596 <https://doi.org/10.1029/2010JA015461>
- 597 Millward, G. H., I. C. F. Müller-Wodrag, A. D. Aylward, T. J. Fuller-Rowell, A. D. Richmond,
598 and R. J. Moffett, (2001), An investigation into the influence of tidal forcing on F region
599 equatorial vertical ion drift using a global ionosphere-thermosphere model with coupled
600 electrodynamics, *J. Geophys. Res.*, 106, 24,733–24,744, doi:10.1029/2000JA000342.
- 601 Newell, P. T., T. Sotirelis, and S. Wing (2009), Diffuse, monoenergetic, and broadband aurora:
602 The global precipitation budget, *J. Geophys. Res.*, 114, A09207, doi: 10.1029/2009JA014326.
603
- 604 Newell, P.T., and J.W. Gjerloev (2011), Substorm and magnetosphere characteristic scales
605 inferred from the SuperMAG auroral electrojet indices, *J. Geophys. Res.*, 116, A12232,
606 doi:10.1029/2011JA016936.
- 607 Rastätter, L., et al., (2016), GEM-CEDAR Challenge: Poynting Flux at DMSP and modeled
608 Joule Heat, *Space Weather*, 14, 113–135, doi:10.1002/2015SW001238.
- 609 Reinisch, B., and I. Galkin, (2011). Global Ionospheric Radio Observatory (GIRO). *Earth,*
610 *Planets, and Space*. 63. 377-381. 10.5047/eps.2011.03.001.

- 611 Richmond, A. D., E. C. Ridley and R. G. Roble, (1992), A Thermosphere/Ionosphere General
612 Circulation Model with coupled electrodynamics, *Geophys. Res. Lett.*, **19**, 601-604.
- 613 Rideout, W., and A. Coster, (2006), Automated GPS processing for global total electron content
614 data, GPS Solution, doi:10.1007/s10291-006-0029-5.
- 615 Ridley, A. J., Y. Deng, and G. Toth, (2006), The global ionosphere-thermosphere model, *J.*
616 *Atmos. Sol. Terr. Phys.*, **68**, 839-864.
- 617 Roble, R. G., E. C. Ridley, A. D. Richmond, and R. E. Dickinson, (1988), A coupled
618 thermosphere/ionosphere general circulation model, *Geophys. Res. Lett.*, **15**, 1325–1328,
619 doi:10.1029/GL015i012p01325.
- 620 Scherliess, L., Tsagouri, I., Yizengaw, E., Bruinsma, S., Shim, J. S., Coster, A., and Retterer, J.
621 M. (2019). The International Community Coordinated Modeling Center space weather modeling
622 capabilities assessment: Overview of ionosphere/thermosphere activities. *Space Weather*, **17**.
623 [https:// doi.org/10.1029/2018SW002036](https://doi.org/10.1029/2018SW002036)
- 624 Schunk, R. W., Scherliess, L., Eccles, V., Gardner, L. C., Sojka, J. J., Zhu, L., et al. (2021).
625 Challenges in specifying and predicting space weather. *Space Weather*, **19**, e2019SW002404.
626 [https:// doi.org/10.1029/2019SW002404](https://doi.org/10.1029/2019SW002404)
- 627 Shim, J. S., et al., (2011), CEDAR Electrodynamics Thermosphere Ionosphere (ETI) Challenge
628 for systematic assessment of ionosphere/thermosphere models: NmF2, hmF2, and vertical drift
629 using ground-based observations, *Space Weather*, **9**, S12003, doi:10.1029/2011SW000727.

630 Shim, J. S., et al., (2012), CEDAR Electrodynamic Thermosphere Ionosphere (ETI) Challenge
631 for systematic assessment of ionosphere/thermosphere models: Electron density, neutral density,
632 NmF2, and hmF2 using space based observations, *Space Weather*, 10, S10004,
633 doi:10.1029/2012SW000851.

634 Shim, J. S., et al., (2014), Systematic Evaluation of Ionosphere/Thermosphere (IT) Models:
635 CEDAR Electrodynamic Thermosphere Ionosphere (ETI) Challenge (2009-2010), in *Modeling*
636 *the Ionosphere-Thermosphere System*, AGU Geophysical Monograph Series.

637 Shim, J. S., Rastätter, L., Kuznetsova, M., Bilitza, D., Codrescu, M., Coster, A. J., ... Zhu, L.
638 (2017a). CEDAR-GEM challenge for systematic assessment of Ionosphere/thermosphere models
639 in predicting TEC during the 2006 December storm event. *Space Weather*, 15, 1238–1256.
640 <https://doi.org/10.1002/2017SW001649>

641

642 Shim, J. S., G. Jee, and L. Scherliess (2017b), Climatology of plasmaspheric total electron
643 content obtained from Jason 1 satellite, *J. Geophys. Res. Space Physics*, 122, 1611–1623,
644 doi:10.1002/2016JA023444.

645

646 Shim, J. S., Tsagouri, I., Goncharenko, L., Rastaetter, L., Kuznetsova, M., Bilitza, D., et al.
647 (2018). Validation of ionospheric specifications during geomagnetic storms: TEC and foF2
648 during the 2013 March storm event. *Space Weather*, 16, 1686–1701. [https://doi.org/10.1029/](https://doi.org/10.1029/2018SW002034)
649 [2018SW002034](https://doi.org/10.1029/2018SW002034)

650

- 651 Solomon, S. C., A. G. Burns, B. A. Emery, M. G. Mlynczak, L. Qian, W. Wang, D. R. Weimer,
652 and M. Wiltberger (2012). Modeling studies of the impact of high-speed streams and co-rotating
653 interaction regions on the thermosphere-ionosphere. *J. Geophys. Res.*, *117*, A00L11,
654 doi:10.1029/2011JA017417
- 655 Sorathia, K., Merkin, V., Panov, E., Zhang, B., Lyon, J., Garretson, J., et al. (2020). Ballooning-
656 interchange instability in the near-Earth plasma sheet and auroral beads: Global magnetospheric
657 modeling at the limit of the MHD approximation. *Geophysical Research Letters*, *47*(14),
658 e2020GL088227. <https://doi.org/10.1029/2020GL088227>
- 659 Tsagouri, I., Goncharenko, L., Shim, J. S., Belehaki, A., Buresova, D., & Kuznetsova, M.
660 (2018). Assessment of current capabilities in modeling the ionospheric climatology for space
661 weather applications: foF2 and hmF2. *Space Weather*, *16*, 1930–1945.
662 <https://doi.org/10.1029/2018SW002035>
- 663 Toffoletto, F., Sazykin, S., Spiro, R., & Wolf, R. (2003). Inner magnetospheric modeling with
664 the rice convection model. *Space Science Reviews*, *107*(1–2), 175–196.
665 <https://doi.org/10.1023/A:1025532008047>
- 666 Webb, P. A., M. M. Kuznetsova, M. Hesse, L. Rastaetter, and A. Chulaki, (2009), Ionosphere-
667 thermosphere models at the Community Coordinated Modeling Center, *Radio Sci.*, *44*, RS0A34,
668 doi:10.1029/2008RS004108.
- 669 Weimer, D. R., (2005), Improved ionospheric electrodynamic models and application to
670 calculating Joule heating rates, *J. Geophys. Res.*, *110*, A05306, doi:10.1029/2004JA010884.

671 Zhang, B., Sorathia, K. A., Lyon, J. G., Merkin, V. G., Garretson, J. S., & Wiltberger, M. (2019).
672 GAMERA: A three-dimensional finite-volume MHD solver for non-orthogonal curvilinear
673 geometries. *The Astrophysical Journal Supplement Series*, 244(1), 20.
674 <https://doi.org/10.3847/1538-4365/ab3a4c>

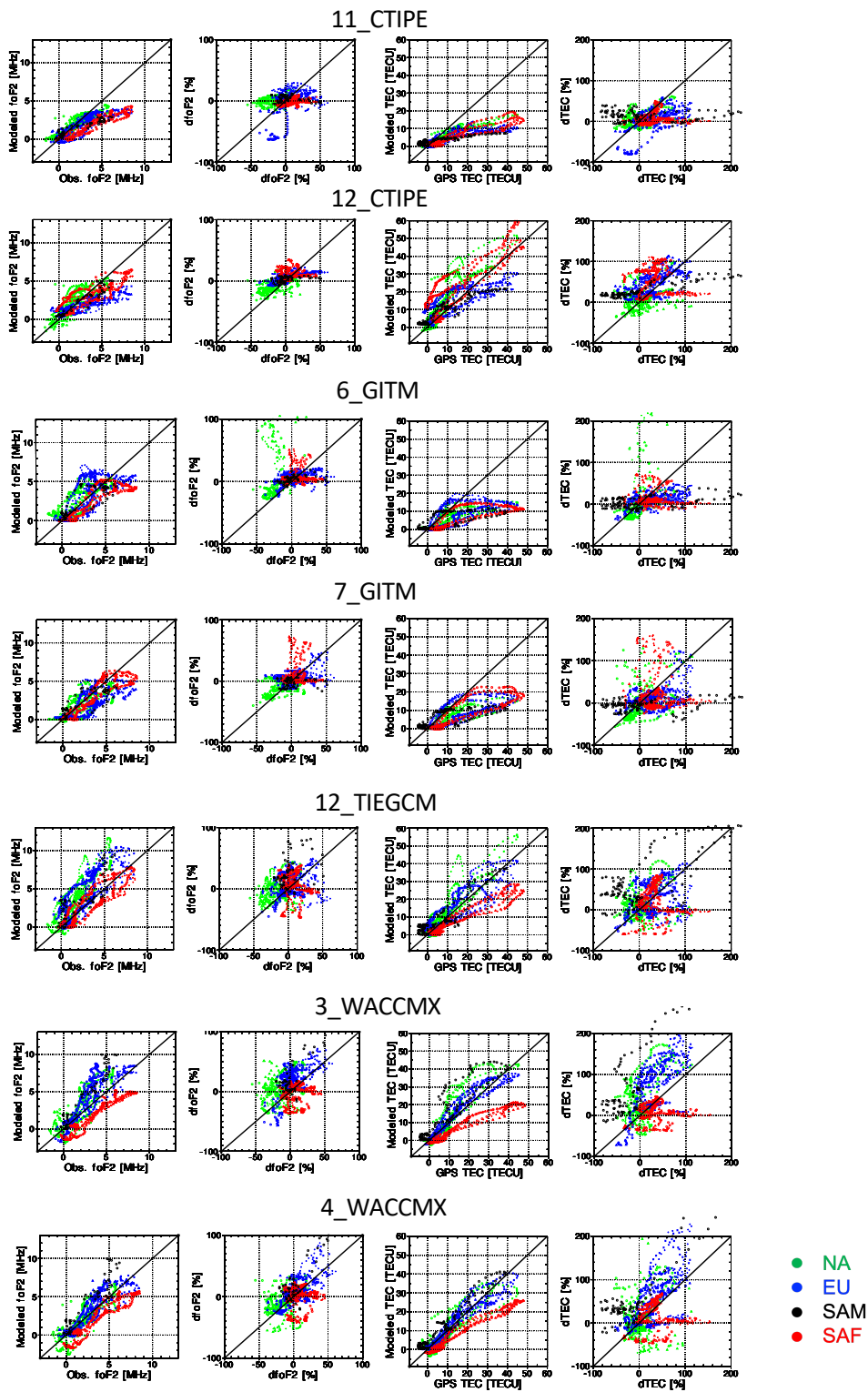


Figure 1

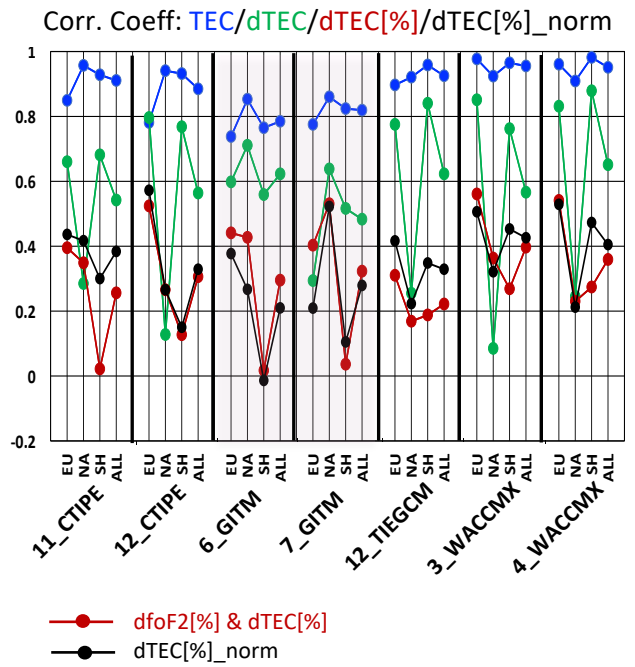
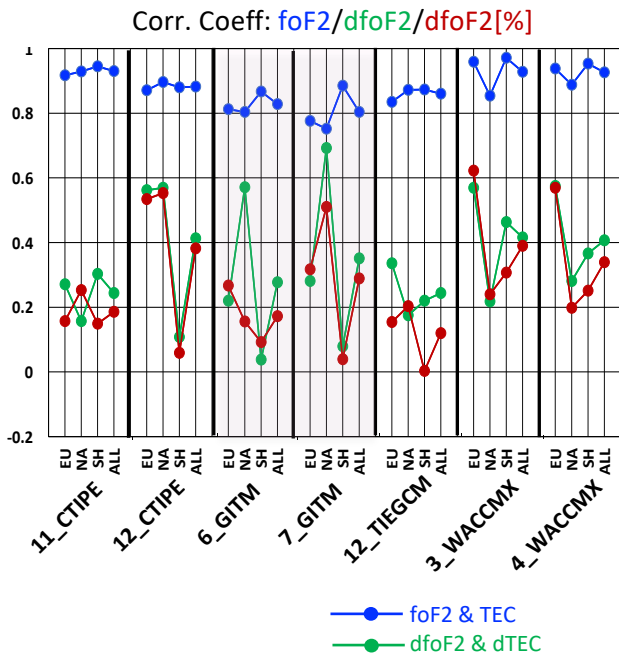
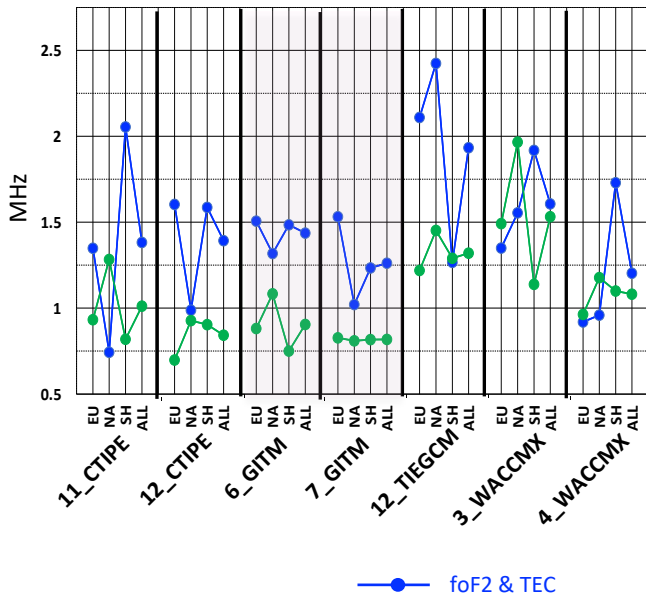


Figure 2

RMSE: foF2/dfoF2



RMSE: TEC/dTEC

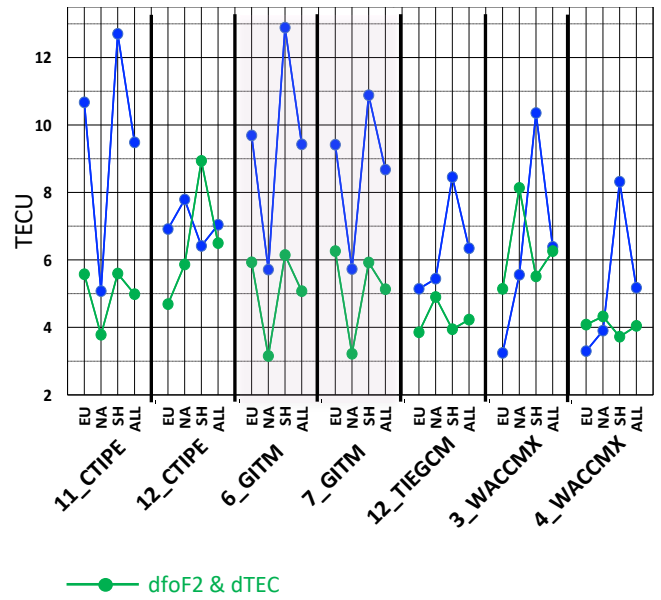


Figure 3

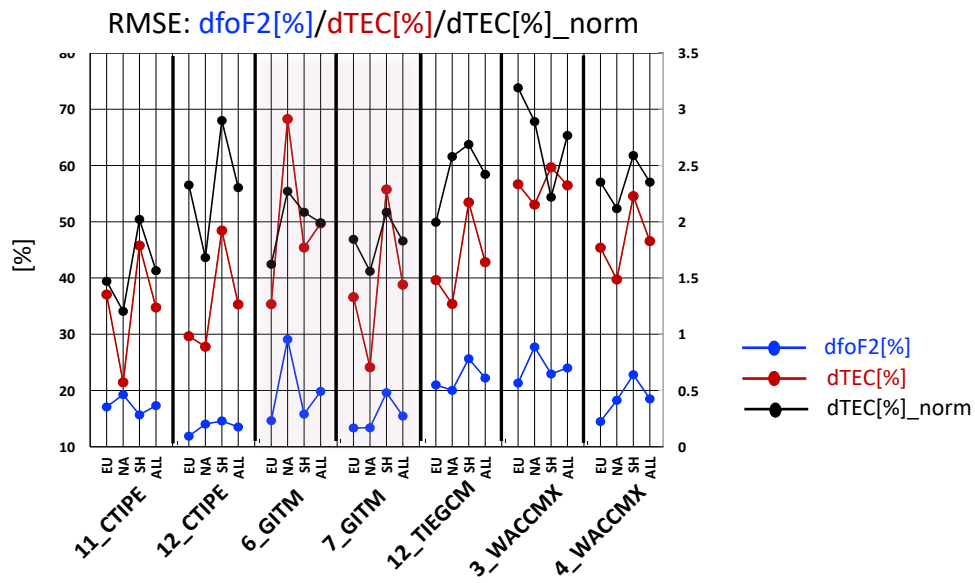


Figure 4

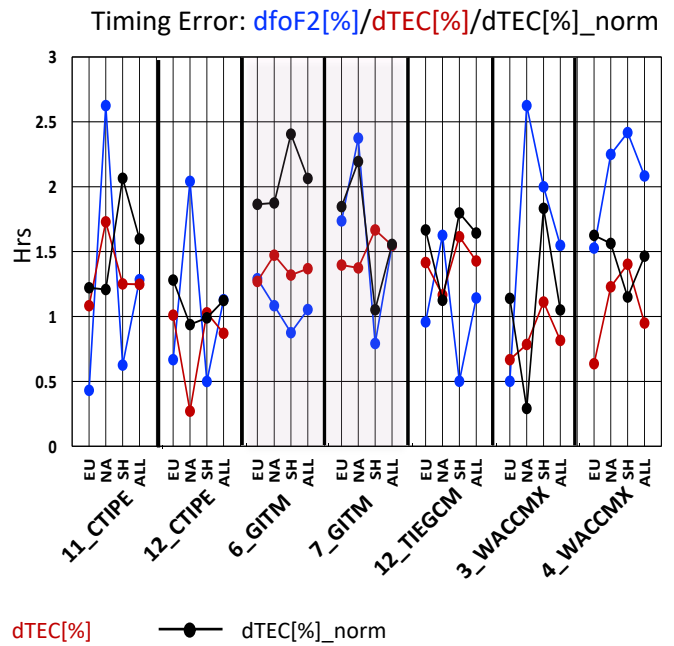
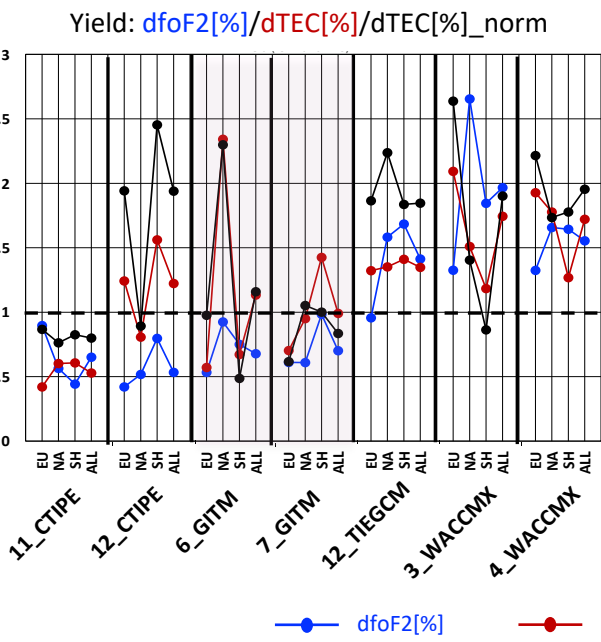


Figure 5

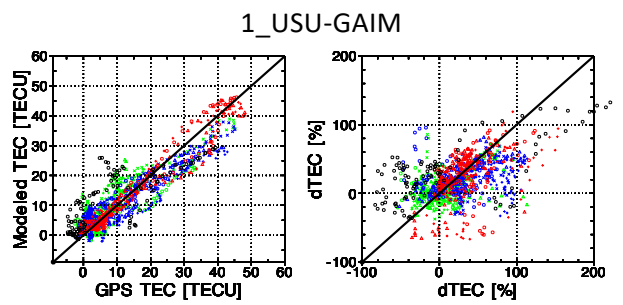
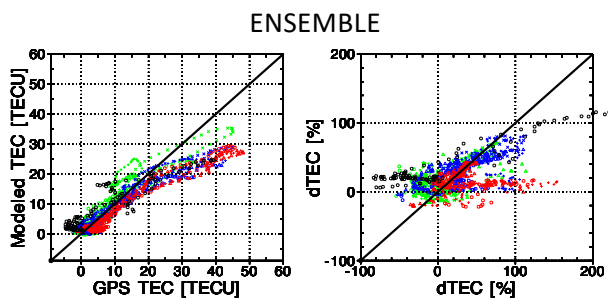


Figure 6

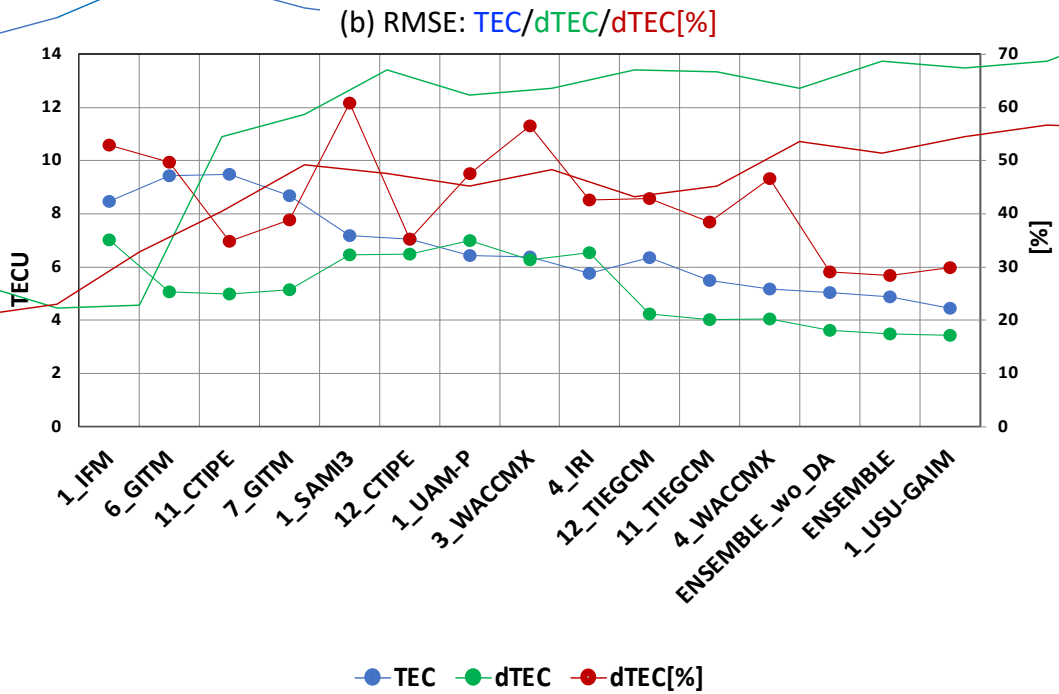
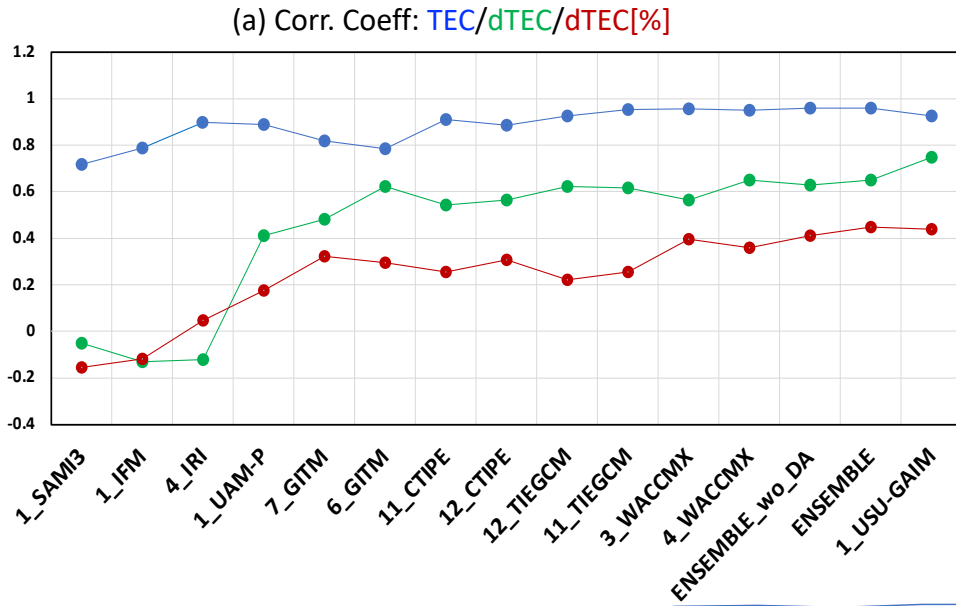


Figure 7

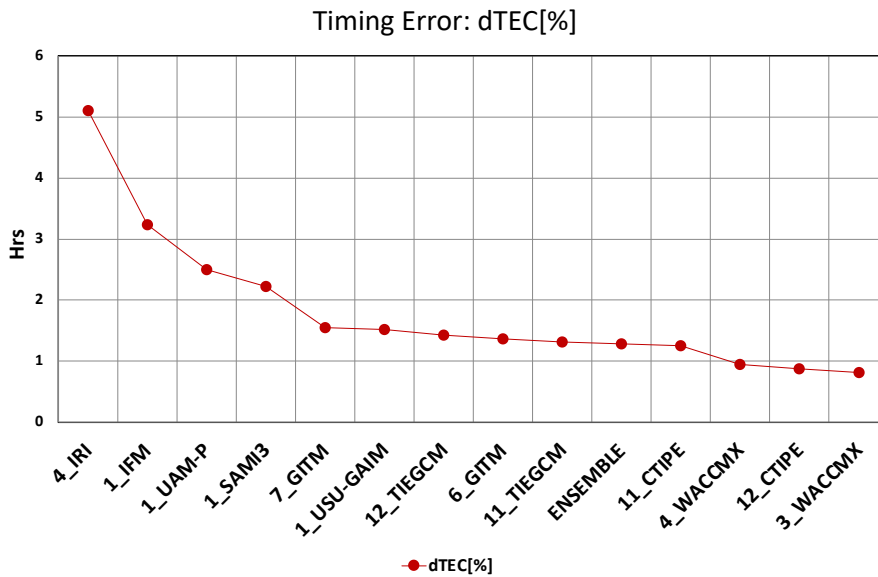
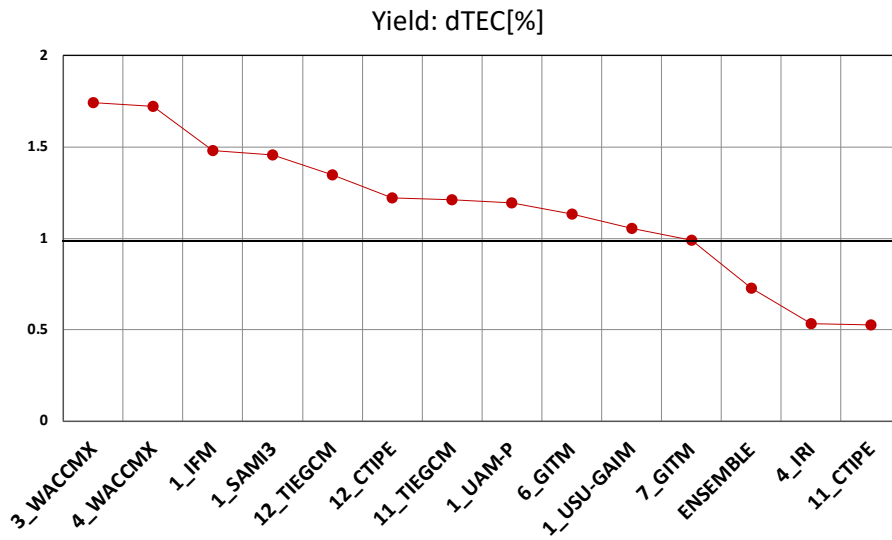


Figure 8

17 Figure 1. Scatter plots of the observed (x axis) and modeled (y axis) shifted foF2 and TEC (foF2*
18 in the 1st, TEC* in the 3rd columns), and percentage change of foF2 and TEC (dfoF2[%] in the
19 2nd, dTEC[%] in the 4th columns) during the storm (03/17/2013) for all 12 locations grouped into
20 North America (NA, green), Europe (EU, blue), South Africa (SAF, red), and South America
21 (SAM, black)

22

23 Figure 2. Correlation Coefficients (CC) between modeled and observed foF2 (left panel) and
24 TEC (right panel). Four CCs are displayed for each simulation: CC averaged over Europe (EU),
25 North America (NA), Southern Hemisphere (SH refers to SAF and SAM combined), and all 12
26 locations, from left to right. Different colors denote different quantities. Blue denotes shifted
27 foF2 and TEC, green and red the change and percentage changes, and black normalized
28 percentage change. The closer the circles are to the horizontal line of 1, the better the model
29 performances are.

30

31 Figure 3. Same as Figure 2 but for RMSE of shifted foF2 and TEC, and changes of foF2 and
32 TEC

33

34 Figure 4. Same as Figure 2 but for RMSE of percentage change of foF2 and TEC, and
35 normalized percentage change. Blue denotes dfoF2[%], red and black dTEC[%] and
36 dTEC[%]_norm.

37

38 Figure 5. Same as Figure 2 but for Yield (ratio) and absolute of Timing Error ($|TE| =$
39 $|t_{\text{peak_model}} - t_{\text{peak_obs}}|$)

40

41 Figure 6. Same as Figure 1 but for only TEC and dTEC[%] from the ensemble of the simulations
42 (ENSEMBLE) and 1_USU-GAIM

43

44 Figure 7. Averaged CC (a) and RMSE (b) over all 12 locations of 13 simulations, the ensemble
45 of them (ENSEMBLE), and the ensemble of 12 simulations excluding 1_USU-GAIM
46 (ENSEMBLE_wo_DA). Blue denotes shifted TEC, green and red the change and percentage
47 changes of TEC. CCs are plotted from the smallest to the largest (closer to 1) according to the
48 average of the three averaged CC values of TEC, dTEC and dTEC[%]. RMSEs are plotted from
49 the largest to the smallest according to the average RMSE for TEC and dTEC.

50

51 Figure 8. Yield and Timing Error of dTEC[%] for all 13 simulations and ENSEMBLE.

52

1 Table 1. Quantities and Skill Scores for Model-Data Comparison

| Quantities and skill scores for model-data comparison | |
|---|--|
| Quiet time references | 30-day median value at a given time: TEC_quiet(UT), 30 days consist of 15 days before (03/01-03/15/2013) and 15 days after (03/22-04/05/2013) the storm |
| Shifted TEC/foF2: | e.g., TEC*(doy, UT) = TEC(doy, UT) – minimum of TEC_quiet(UT) |
| TEC/foF2 changes w.r.t. the quiet time | e.g., dTEC(doy, UT) = TEC(doy, UT) – TEC_quiet(UT) |
| TEC/foF2 percentage changes w.r.t. the quiet time | e.g., dTEC[%](doy, UT) = 100 * dTEC(doy, UT) / TEC_quiet(UT) |
| Normalized Percentage changes of TEC | dTEC[%]_norm = (dTEC[%] - ave_dTEC[%]) / std_dTEC[%]; ave_dTEC[%] is the average of dTEC[%] at a given time and at a given location over the quiet 30 days, std_dTEC[%] is the standard deviation of the average percentage change |
| Skill Scores | |
| CC | Correlation Coefficient |
| RMSE | Root-Mean-Square Error ($= \sqrt{\frac{\sum(x_{obs} - x_{mod})^2}{N}}$), where x_{obs} and x_{mod} are observed and modeled values |
| Yield | ratio of the peak of modeled percentage change to that of the observed one ($= \frac{(x_{mod})_{max}}{(x_{obs})_{max}}$) |
| Timing Error (TE) | difference between the modeled peak time and observed peak time: TE = t_peak_model – t_peak_obs |

2

3

4

5

6

7 Table 2. Models used for this study

| Model Setting ID | Model Version | Drivers | | Upper boundary for TEC calculation/ Resolution |
|---|---|--|---|--|
| | | Input data | Models used for thermosphere, tides from lower boundary, and high latitude electrodynamics | |
| Physics-based Coupled Ionosphere-Thermosphere Model | | | | |
| | | | Tides | High Latitude Electrodynamics |
| 11_CTIPE ^a | CTIPe3.2 [<i>Codrescu et al.</i> , 2000; <i>Milward et al.</i> , 2001] | F10.7, ACE IMF data and solar wind speed and density, NOAA POES Hemispheric Power data | (2,2), (2,3), (2,4), (2,5), and (1,1) propagating tidal modes | Weimer-2005 high latitude electric potential [<i>Weimer</i> , 2005], Fuller-Rowell and Evans auroral precipitation [1987] |
| 12_CTIPE ^a | CTIPe4.1 | | WAM [<i>Akmaev et al.</i> , 2011, <i>Fuller-Rowell et al.</i> , 2010] tides | |
| 6_GITM ^a | GITM2.5 [<i>Ridley et al.</i> , 2006] | FISM solar EUV irradiance, ACE IMF data and solar wind speed and density | MSIS [<i>Hedin</i> , 1991] migrating diurnal and semidiurnal tides | Weimer-2005 high latitude electric potential, Ovation auroral precipitation [<i>Newell et al.</i> , 2009; 2011] |
| 7_GITM | GITM21.11 | | | Weimer-2005 high latitude electric potential, Fang's auroral precipitation [<i>Fang et al.</i> , 2013] |
| 12_TIE-GCM ^a | TIE-GCM2.0 [<i>Roble et al.</i> , 1988; <i>Richmond et al.</i> , 1992; <i>Solomon et al.</i> , 2012] | F10.7, Kp, OMNI IMF data and solar wind speed and density | GSWM [<i>Hagan et al.</i> , 1999] migrating diurnal and semidiurnal tides | Weimer-2005 high latitude electric potential, Roble and Ridley auroral precipitation [1987] |
| Whole Atmosphere Model | | | | |
| 3_WACCM-X | CESM2.2 [<i>Gottelman et al.</i> , 2019; <i>Liu et al.</i> , 2018] | F10.7, Kp, OMNI IMF data and solar wind speed and density | Heelis high latitude electric potential [<i>Heelis et al.</i> , 1982], Roble and Ridley auroral precipitation [1987] | ~600 km, 1.9° lat. × 2.5° long. |
| 4_WACCM-X | | | Weimer-2005 high latitude electric potential, Roble and Ridley auroral precipitation [1987] | |

8 ^aThe model results are submitted by the CCMC using the models hosted at the CCMC

10 Table 3. Number of locations where the models correctly predict negative or positive phase.

| | Time Interval | 11_CTIPE | 12_CTIPE | 6_GITM | 7_GITM | 12_TIE-GCM | 3_WACCM-X | 4_WACCM-X |
|----------|---------------|-----------|-----------|-----------|-----------|------------|-----------|-----------|
| dfoF2[%] | 06–15UT | 8 | 7 | 5 | 9 | 9 | 6 | 10 |
| | 15–22UT | 10 | 6 | 7 | 8 | 7 | 7 | 10 |
| dTEC[%] | 06–15UT | 9 | 10 | 10 | 10 | 7 | 10 | 9 |
| | 15–22UT | 7 | 10 | 12 | 11 | 10 | 7 | 8 |

11

12 Table 4. Averaged RMSE over all 12 locations of the ensemble of newer versions (ENSEMBLE_new) of models (12_CTIPE, 7_GITM and
 13 4_WACCM-X) driven by Weimer2005 electric potential model, the ensemble of older versions (ENSEMBLE_old) of models (11_CTIPE,
 14 6_GITM and 12_TIE-GCM), and 1_USU-GAIM.

| | TEC (TECU) | dTEC (TECU) | dTEC[%] |
|--------------|------------|-------------|---------|
| ENSEMBLE_old | 6.6 | 4.1 | 33.4 |
| ENSEMBLE_new | 4.6 | 3.2 | 29.8 |
| 1_USU-GAIM | 4.5 | 3.4 | 29.9 |

15

16

Validation of Ionospheric Specifications During Geomagnetic Storms: TEC and foF2 during the 2013 March Storm Event-II

J. S. Shim¹, I.-S. Song¹, G. Jee², Y.-S. Kwak³, I. Tsagouri⁴, L. Goncharenko⁵, J. McInerney⁶, A. Vitt⁶, L. Rastaetter⁷, J. Yue^{7,8}, M. Chou^{7,8}, M. Codrescu⁹, A. J. Coster⁵, M. Fedrizzi⁹, T. J. Fuller-Rowell⁹, A. J. Ridley¹⁰, S. C. Solomon⁶

¹Department of Atmospheric Sciences, Yonsei University, Seoul, South Korea,

²Division of Atmospheric Sciences, Korea Polar Research Institute, Incheon, South Korea

³Space Science Division, Korea Astronomy and Space Science Institute, Daejeon, South Korea

⁴National Observatory of Athens, Penteli, Greece,

⁵Haystack Observatory, Westford, MA, USA,

⁶High Altitude Observatory, NCAR, Boulder, CO, USA,

⁷NASA GSFC, Greenbelt, MD, USA,

⁸Catholic University of America, Washington, DC, USA,

⁹NOAA SWPC, Boulder, CO, USA,

¹⁰Space Physics Research Laboratory, Univ. of Michigan, Ann Arbor, MI, USA

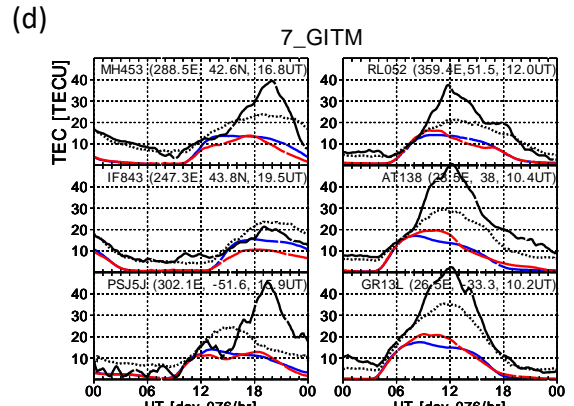
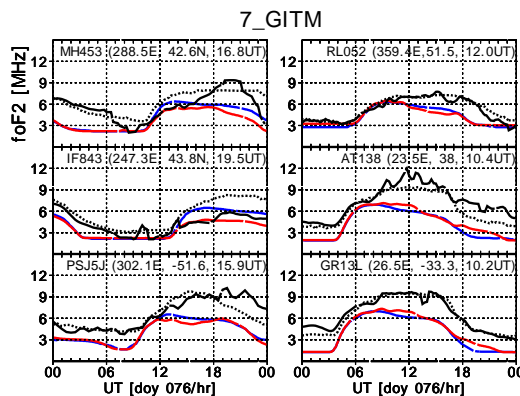
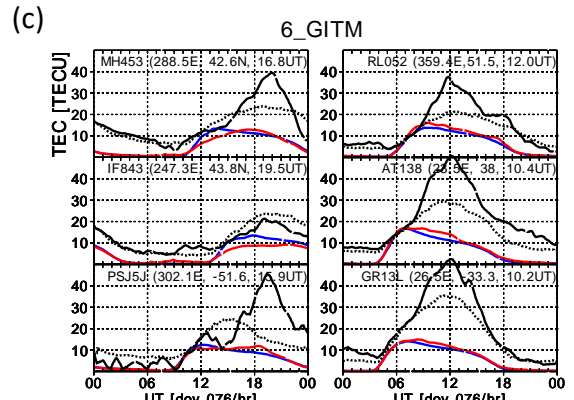
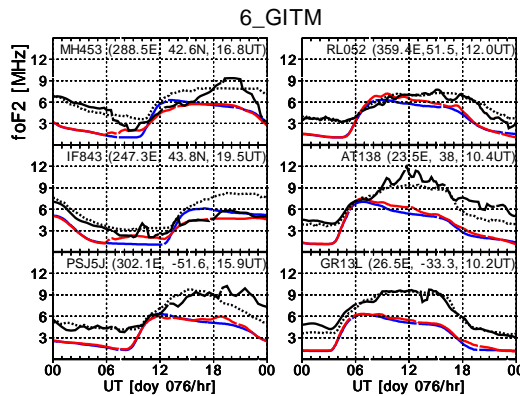
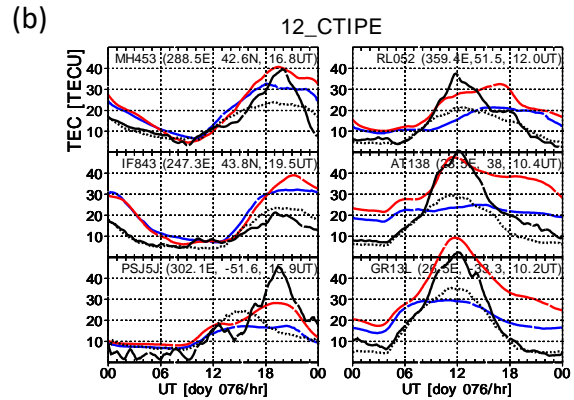
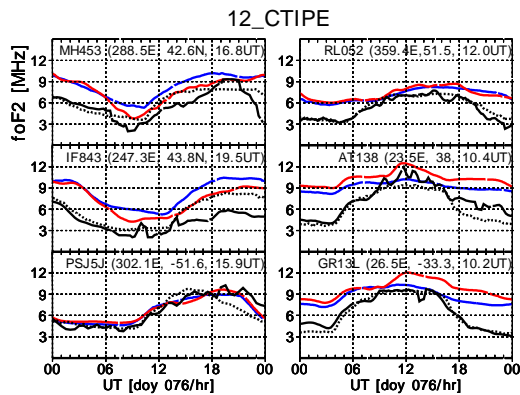
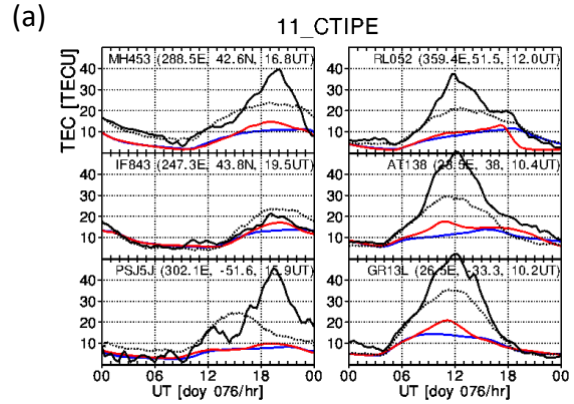
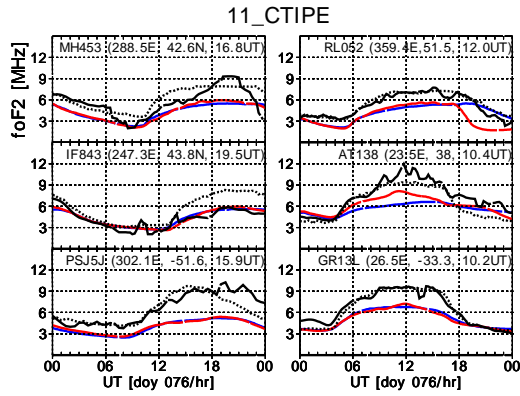
Contents of this file

Figures S1

Introduction

This supporting information file includes:

1. Figure S1: Comparison foF2 and TEC data with modeled values



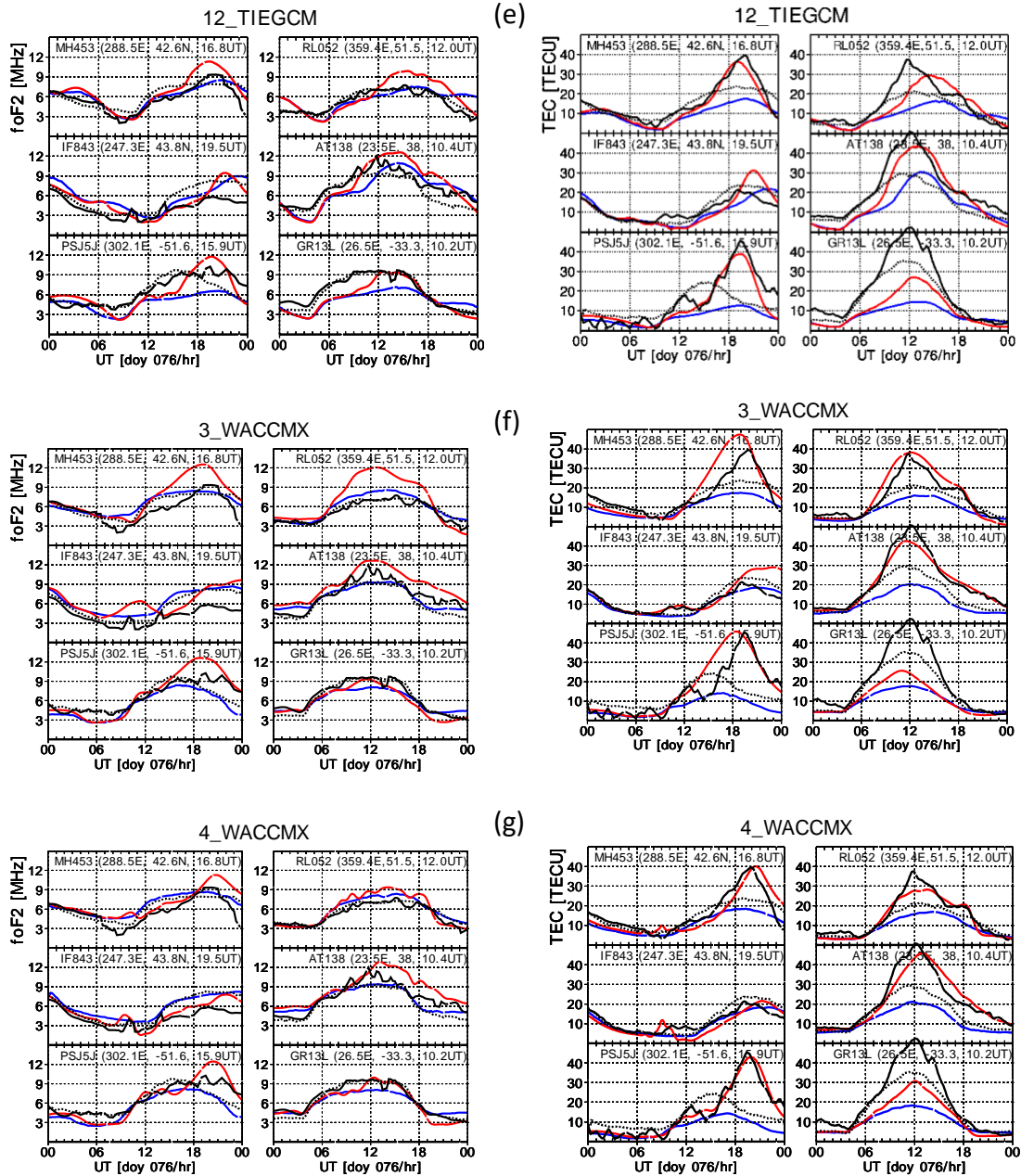


Figure S1. Comparison foF2 and TEC data with modeled values: (a) 11_CTIGE, (b) 12_CTIGE, (c) 6_GITM, (d) 7_GITM, (e) 12_TIEGCM, (f) 3_WACCM-X, and (g) 4_WACCM-X. In each plot, foF2 in the first two columns and TEC in the other two. Black solid and dotted lines denote observed storm time values and quiet-time reference (30-day median) respectively. Red and blue curves denote modeled storm time values and 30-day median.